

1 **Global warming will largely increase waste treatment CH₄ emissions in Chinese Megacities:**
2 **insight from the first city scale CH₄ concentration observation network in Hangzhou city,**
3 **China**

4
5 Cheng Hu^{1,2}, Junqing Zhang¹, Bing Qi^{3,4*}, Rongguang Du^{3*}, Xiaofei Xu⁴, Haoyu Xiong⁵, Huili
6 Liu¹, Xinyue Ai¹, Yiyi Peng¹, Wei Xiao²

7 ¹ College of Biology and the Environment, Joint Center for sustainable Forestry in Southern China,
8 Nanjing Forestry University, Nanjing 210037, China

9 ² Collaborative Innovation Center on Forecast and Evaluation of Meteorological Disasters
10 (CIC-FEMD), Nanjing University of Information Science & Technology, Nanjing, China

11 ³ Hangzhou meteorological bureau, Hangzhou 310051, China

12 ⁴ Zhejiang Lin'an Atmospheric Background National Observation and Research Station, Hangzhou
13 311300, China

14 ⁵ College of Environment, Zhejiang University of Technology, Hangzhou 311300, China

15

16

17

18

19

20

21

22 *Corresponding authors: Bing Qi (bill_129@sina.com), Rongguang Du (drg1998@163.com).

23

24

25

26

27

28

29 To be submitted to: *ACP*

30

31

32

33 **Abstract:**

34 Atmospheric CH₄ is the second largest anthropogenic contributor to global warming. However, its emissions,
35 components, spatial-temporal variations and projected changes still remain largely uncertain from city to national
36 scales. CH₄ emissions from waste treatment (including solid waste landfills, solid waste incineration and sewage)
37 account for >50% of total anthropogenic CH₄ emissions at city scale, and considering the high temperature
38 sensitivity of CH₄ emission factors (EFs) for the biological processes-based sources such as waste treatment, large
39 differences will be caused when estimating future CH₄ emissions under different global warming scenarios.
40 Furthermore, the relationships between temperature and waste treatment CH₄ emissions have only been studied in
41 a few site-specific studies and lack the representativity for whole city, which contains various biophysical
42 conditions and shows heterogeneous distribution. The above factors cause uncertainty in the evaluation of city
43 scale CH₄ emissions (especially from waste treatments) and projected changes still remain unexplored. Here we
44 conduct the first tower-based CH₄ observation network with three sites in Hangzhou city, which is located in
45 developed Yangtze River Delta (YRD) area and ranks as one of the largest megacities in China. We found the *a*
46 *priori* total annual anthropogenic CH₄ emissions and those from waste treatment were overestimated by 36.0% and
47 47.1% in Hangzhou city, respectively. In contrast, the total emissions in the larger region, such as Zhejiang
48 province or the YRD area, were slightly underestimated by 7.0%. Emissions from waste treatment showed obvious
49 seasonal patterns following air temperature. By using the linear relationship constructed between monthly waste
50 treatment CH₄ emissions and air temperature, we find the waste treatment EFs increase by 38%~50% with
51 temperature increases of 10°C. Together with projected temperature changes from four climate change scenarios,
52 the global warming induced EFs in Hangzhou city will increase at the rates of 2.2%, 1.2%, 0.7% and 0.5% per
53 decade for IPCC AR5 (International Peace Cooperation Center, the fifth assessment report) RCP (Representative
54 Concentration Pathway)8.5, RCP6.0, RCP4.5 and RCP2.6 scenarios, respectively. And the EFs will finally
55 increase by 17.6%, 9.6%, 5.6%, and 4.0% at the end of this century. Additionally, the derived relative changes in
56 China also show high heterogeneity and indicate large uncertainty in projecting future national total CH₄ emissions.
57 Hence, we strongly suggest the temperature-dependent EFs and the positive feedback between global warming and
58 CH₄ emissions should be considered in future CH₄ emission projections and climate change models.

59 **Keyword:** CH₄ emissions, waste treatment, observation network, global warming

60

61

62 **1. Introduction**

63 As the second largest anthropogenic greenhouse gas, the reduction of CH₄ emissions is considered
64 an effective way to mitigate future climate change on short timescales (Henne et al., 2016; Lin et
65 al., 2021). Accurate estimation of CH₄ emissions from its main sources is the basis of policy
66 making. However, recent studies find there still remain large uncertainties for its total emissions,
67 components, spatial-temporal variations and projected changes at city scale especially for
68 megacities in China (USPA 2013; Cai et al., 2018; Lin et al., 2021). CH₄ emission from waste
69 treatment (mainly including sewage and solid waste by landfills and incineration) ranked as the
70 world's third largest anthropogenic source after fuel exploitation and livestock, and was
71 responsible for ~13% of global anthropogenic CH₄ emissions of 371 (±26) Tg a⁻¹ (Lu et al., 2021).
72 It also ranked as the fourth largest anthropogenic source in China, the biggest anthropogenic CH₄
73 emitting country, and accounted for ~14% of national total anthropogenic emissions of 65 (±22)
74 Tg a⁻¹ (Saunois et al., 2020; Lu et al., 2021; Chen et al., 2022). Furthermore, its contribution is
75 even larger than 50% at city scale especially for megacities, where both active and closed
76 household waste (including landfills and waste water systems) are located and found as super
77 emitters (Williams et al., 2022; Maasakkers et al., 2022). A large number of Chinese landfills were
78 constructed in suburbs more than 5-10 years ago and most landfills have no gas collection systems,
79 with the urban area expanding in recent decades, the locations of many landfills are now within
80 the urban scope (Zhejiang Statistical Yearbook 2018-2019). In addition, the decreasing area of the
81 agricultural sector (rice paddies and husbandry) in megacities also makes their emissions
82 negligible when compared with waste treatment. Therefore, accurate quantification of CH₄
83 emissions from waste treatment in urban area becomes increasingly important.

84

85 Although some progress has been made in measuring site scale CH₄ emissions from waste
86 treatment, the estimated emissions still show large discrepancies due to many factors such as the
87 amount of waste and its composition, relative proportions of landfills and incineration, degradable
88 organic carbon ratio, CH₄ oxidation efficiency, and landfill gas collection, and meteorological
89 conditions including temperature, water content, atmospheric pressure (Masuda et al., 2018; Cai et
90 al., 2018; Zhao et al., 2019; Hua et al., 2022; Bian et al., 2022; Maasakkers et al., 2022; Kissas et

91 al., 2022).

92

93 Furthermore, CH₄ emissions from sewage and landfills result from microbial processes especially
94 from methanogens, and their emission factors (EFs) are highly sensitive to temperature. These
95 available studies were mainly conducted at some specific sites with measured EFs varying widely
96 (Du et al., 2017; 2018; Cai et al., 2014; 2018; Zhao et al., 2019; NBSC, 2015; Wang et al., 2015;
97 Florentino et al., 2010; Tolaymat et al., 2010; Hua et al., 2022). The lack and discrepancies of
98 detailed information for all the above factors and their uncertainties have led to considerable
99 difficulty in estimating CH₄ emissions for most-to-date inventories (Höglund-Isaksson, 2012;
100 USEPA et al., 2013; Cai et al., 2018; Lin et al., 2021; Maasakkers et al., 2022).

101

102 China, the developing country with the largest anthropogenic CH₄ emissions, is expected to
103 increase its emissions because of projected rapid economic development, urbanization and
104 generated waste (Cai et al., 2018). The increase of waste treatment emissions in East China was
105 also found as the second largest sector in driving national total anthropogenic CH₄ emissions since
106 2000 (Lin et al., 2021). In addition, the mitigation potential of waste treatment in developing
107 countries is thought to be four times that of developed countries (USEPA, 2013). Therefore,
108 mitigating CH₄ emissions from waste treatment in China is a robust and cost-effective way to
109 reduce total national anthropogenic greenhouse gas emissions.

110

111 Many previous studies have estimated the waste treatment CH₄ emissions for China by both
112 “bottom-up” and “top-down” approaches, with results varied by 2.5-fold from 4.3 to 10.4 Tg CH₄
113 yr⁻¹, and accounted for 8.1%~24.2% of national total anthropogenic CH₄ emissions (USEPA 2013;
114 Peng et al., 2016; Miller et al., 2019; Lin et al., 2021; Lu et al., 2021; Chen et al., 2022). For these
115 “bottom-up” approaches, the high uncertainties were directly attributed to omission of many small
116 point sources and discrepancies of observed site-specific EFs, which varied largely by climate and
117 management technology such as the efficiency of gas collection systems (Zhao et al., 2019; Hua et
118 al., 2022). Previous studies most commonly used the EDGAR (Emission Database for Global
119 Atmospheric Research) inventory, using the IPCC recommended default EF values of 15.0%

120 (Höglund-Isaksson, 2012; Lin et al., 2021; Bian et al., 2022), but this value is around 5-7 times
121 higher than those used EFs in China by Zhang and Chen et al. (2014). A recent study comparing
122 waste treatment CH₄ emissions among different inventories also reported that the EDGAR v5.0
123 and CEDS (Community Emissions Data System) inventories were 21~153% higher than other
124 inventories, and EDGAR v5.0 tended to assign more emissions in urban areas especially for
125 provincial capitals. In addition, emissions from wastewater were found to be overestimated by
126 higher emission factors or chemical oxygen demand (Peng et al., 2016; Lin et al., 2021).

127

128 And for the “top-down” atmospheric inversion approaches, a few studies constrained
129 anthropogenic sources including waste treatment, where the most widely used concentrations were
130 from satellite observations (Miller et al., 2019; Lu et al., 2021; Chen et al., 2022). The satellite
131 observations have the advantage of easy data access and global coverage. But as already noted, the
132 emissions constraint results are highly dependent on availability of observed concentrations,
133 which are largely influenced by weather conditions and cloud coverage. As was illustrated in a
134 recently published study by Chen et al. (2022), although the numbers of grid cell (0.25° × 0.3125°)
135 based year-round satellite observations were more than 1000 in north China, the available
136 numbers of satellite observations were less than 10 (even including grid cells without any
137 observations) in most of central, west, east and south of China. Such sparse distribution of
138 available data may not provide robust constrains on waste treatment emissions for some Chinese
139 cities without enough observations, especially considering waste treatment is co-located with high
140 population density megacities in the developed area of east and south of China. Furthermore, there
141 should be large temperature induced monthly variations for waste treatment CH₄ emissions
142 (Börjesson et al., 1997), but almost all satellite-based inversions were conducted at annual scale
143 without seasonal variations. Besides, given the strong influence from atmospheric pressure on
144 landfill CH₄ emissions (Kissas et al., 2022), satellite observations are too sparse to be up-scaled to
145 estimate annual total because satellite observations are mostly available only on clear-sky
146 conditions and cannot represent atmospheric pressure and CH₄ emissions on cloudy or rainy days.
147 There was only one recent study which focused on urban waste treatment CH₄ emissions, it found
148 annual CH₄ emissions from four cities were 1.4 to 2.6 times larger than inventories in India and

149 Pakistan, where landfills contributed to 6~50% of total emissions and indicated large bias of our
150 understanding of waste treatment CH₄ emissions (Maasakkers et al., 2022).

151

152 The tower-based atmospheric inversion approach, which is based on hourly atmospheric
153 concentration observations within the planetary boundary layer, can be used independently to
154 constrain CH₄ emissions and its main components. Besides, compared with “bottom-up”
155 approaches, the “top-down” method can avoid using the factors that lead to large uncertainties in
156 CH₄ emissions especially from waste treatment. And to our best knowledge, there are few
157 tower-based observation inversion studies which focus on waste treatment emissions at city scale
158 or much larger regional scales especially in China. Only one study in Los Angeles, U.S.A. used
159 tower-based CH₄ concentration and found the influence of a landfill site closure on CH₄ emissions,
160 which was not included in *a priori* inventory (Yadav et al., 2019). In addition, the influences of
161 global warming on city scale (or higher regional scale) emissions are still unclear and have not
162 been considered in future emission projections (USEPA 2013; Cai et al., 2018). In general,
163 previous studies which predicted future waste treatment CH₄ emissions only used activity data
164 changes, without considering climate change on the EFs. Considering the potential high sensitivity
165 of waste treatment CH₄ emissions on the projected global warming, how these emissions will
166 change with increasing temperature is still unknown, especially within megacities where more
167 waste is generated and the urban heat island effect will lead to much stronger warming climate
168 (Zhang et al., 2022).

169

170 Here, we established three tower-based CH₄ concentration observation sites in Hangzhou city, one
171 of the largest megacities in China. To our best knowledge, it is the first city-scale tower-based CH₄
172 concentration observation network in China. We present our work on urban CH₄ emissions
173 inversion and aim to (1) constrain CH₄ emissions from waste treatment alongside total
174 anthropogenic emissions in Hangzhou city, (2) derive temperature sensitivity of waste treatment
175 CH₄ emissions at city scale and quantify the projected emission changes in future climate change
176 scenarios. One-year hourly CH₄ concentration observations from December 1st, 2020 to
177 November 30th, 2021 were combined with atmospheric transport model and Bayesian inversion

178 approach to constrain monthly CH₄ emission inventories. The constructed relationship between
179 monthly temperature and *posteriori* waste treatment CH₄ emissions will be used with future
180 temperature projection to quantify how the EFs will change in different global warming scenarios.

181

182 **2. Materials and Method**

183 **2.1 Tower-based CH₄ observation network and supplementary materials**

184 The city of Hangzhou, which has a population of 12.2 million and area of 1.7×10^4 km² (core
185 urban area of 8.3×10^3 km²), is the capital of Zhejiang province and located in the middle of East
186 China (Figure 1a). As displayed in Figures S1-S2, East China accounts for the majority of the
187 national total population and waste treatment CH₄ emissions. Hangzhou city ranked in the top 10
188 megacities in China, with annual solid waste of around 5 million tons in 2021. The tower-based
189 CH₄ concentration observation network includes three observation sites (Figure 1a-d), as (1)
190 Hangzhou site (120.17° E, 30.23° N, 43.2 m a.s.l.), which is located in the core urban region; (2)
191 Linan site (119.72° E, 30.30° N, 138.6 m a.s.l.), regional background site with no obvious
192 emission sources within 10 km radius; (3) Damingshan site (119.00° E, 30.03° N, 1485.0 m a.s.l.),
193 which is built on the top of a 1500 m mountain and represents background from much more
194 diluted regional emission signals. The distance is around 50 km between Hangzhou site and Linan
195 site, and around 150 km between Hangzhou site and Damingshan site. These three sites represent
196 obvious gradients from east of densely populated area (Figure 1c-d) and anthropogenic emissions
197 to west of much weaker anthropogenic influence and background conditions. Based on the wind
198 direction for the three sites, there is not any obvious difference of seasonal wind direction patterns
199 among them. The prevailing wind direction from October to February was from the north, which
200 changed to east from February to May and then changed to south during the monsoon in summer.

201

202 The air inlet heights are 25 m above ground for the Hangzhou site, 53 m at Linan and 10 m at
203 Damingshan, respectively. Atmospheric CH₄ concentrations at all three sites were continuously
204 measured by cavity ring-down spectroscopy analyzer (model G2301 for Hangzhou site and G2401
205 for Linan site and Damingshan site; Picarro Inc., Sunnyvale, CA). To obtain high precision
206 observations, two different standard gases were measured every 6 hours and a linear two-point fit

207 was used to calibrate observations, with the precision and accuracy of 2 ppb and 1 ppb. More
208 details of the observation and calibration systems were described in Fang et al., (2014; 2022).
209 Note that because of instrument issues at Damingshan site, there is a data gap in
210 September-October, 2021. In general, 99.4%, 99.0%, 79.3% of hourly CH₄ observations were
211 available in the whole year observation period for Hangzhou site, Linan site and Damingshan site,
212 respectively. Meteorological observations at Hangzhou meteorological station were used to
213 evaluate simulated meteorological fields, including air temperature at 2 m (T_{2m}), relative humidity
214 (RH), downward solar radiation (S↓), wind speed (WS) at 10 m height, and planetary boundary
215 layer height (PBLH).

216

217 Note some previous studies of city scale greenhouse gas concentration observation networks chose
218 sites at the edge of urban borders as background in emission inversion system (i.e. Indianapolis,
219 U.S.A., Miles et al., (2017); Los Angeles, U.S.A., Verhulst et al., (2017); Washington,
220 DC-Baltimore, U.S.A., Lopez-Coto et al., (2020); Paris, France, Lian et al., (2021)), but we chose
221 to use five NOAA CH₄ background sites as the potential background, including UUM, TAP, YRO,
222 YON and WLG site (Figure 1a), which were much further than the observations at Damingshan
223 site. This strategy is based on following three reasons: (1) our footprint domain is much larger
224 than Hangzhou city and these five sites are also located close to the edge of the model domain; (2)
225 CH₄ concentrations within Hangzhou city will be influenced by seasonally varying monsoon and
226 the monthly varying wind directions will lead to obvious changes of CH₄ background than only at
227 Damingshan site; (3) our model setups can partition CH₄ enhancements from within Hangzhou
228 city and other regions.

229

230 The projected climate data from four RCP (Representative Concentration Pathway) scenarios
231 (RCP8.5, RCP6.0, RCP4.5 and RCP2.6) by MRI-CGCM3 model were downloaded from World
232 Data Center for Climate (WDCC, <https://www.wdc-climate.de/ui/>), where annual air temperature
233 at 2m was used from years 2021 to 2100. The most recent population density data for Hangzhou
234 city is for the year 2019 and was downloaded from Chinese national resource and environmental
235 science and data center.

236

237 **2.2 WRF-STILT model setup**

238 The WRF-STILT (WRF: Weather Research and Forecasting, version 4.2.2, and STILT: Stochastic
239 Time-Inverted Lagrangian Transport) model was used to simulate hourly footprint and CH₄
240 enhancement, see more details in Hu et al. (2019; 2021). Domain setups are displayed in Figure 1a,
241 with the outer nested domain (Domain-1, 27 km×27 km grid resolution) covering eastern and
242 central China, and the inner domain (Domain-2, 9 km×9 km grid resolution) covering the YRD
243 area. The physical schemes used in the WRF model are the same as in our previous studies for the
244 YRD domain (Hu et al., 2019; 2021). The simulated CH₄ concentration is the sum of background
245 and enhancement, where the enhancement is calculated by multiplying all CH₄ flux with hourly
246 footprint that represents the sensitivity of the concentration changes to its regional sources/sinks
247 with spatial resolution of 0.1°×0.1°. To better quantify CH₄ components at each site, CH₄
248 enhancements from different regions and sources are also tracked and separately simulated.
249 Besides, we should note the CH₄ background is important in simulating CH₄ concentrations and
250 atmospheric inversion. We will choose CH₄ background from the five background sites based on
251 monthly footprint as discussed in Section 3.1.

252

253 The most recent inventory of Emission Database for Global Atmospheric Research (EDGAR v6.0),
254 which has 20 categories, and WetCHARTs ensemble mean were used as the *a priori*
255 anthropogenic and natural CH₄ emissions. We should note there are many CH₄ inventories for
256 some developed regions and countries (i.e. France, U.S.A., Germany) with high spatial resolutions.
257 The reasons to choose EDGAR as *a priori* anthropogenic emissions are: (1) for all available CH₄
258 inventories that covered China, the spatial resolution of EDGAR (0.1°×0.1°) is the highest, and it
259 provides the most up-to date results; (2) most previous studies that constrain emissions by
260 atmospheric inversion studies also chose EDGAR, and our results can be directly compared with
261 previous studies; (3) the preliminary simulation of CH₄ concentrations showed generally good
262 performance with observations, indicating its spatial distributions in Hangzhou city has relatively
263 small bias even with a potentially large bias for magnitude, which will be constrained by our
264 atmospheric inversion method.

265

266 The main sources of CH₄ emissions in Hangzhou city include SWD_LDF (solid waste landfills),

267 WWT (waste water handling), SWD_INC (solid waste incineration), PRO (all processes related to
 268 fuel exploitation from coal, oil, and natural gas, including extraction, transportation, refining,
 269 distribution as listed in IPCC database (https://www.ipcc-nggip.iges.or.jp/EFDB/find_ef.php),
 270 RCO (energy for buildings, mainly containing natural gas escaping from household use) and AGS
 271 (agricultural soils). We found emissions from SWD_LDF, WWT and SWD_INC were simply
 272 assigned in the same locations in EDGAR inventory, and hence combined them as waste treatment.
 273 For the CH₄ emissions from wetland, we used WetCHARTs ensemble mean with spatial resolution
 274 of 0.5° at monthly average (Bloom et al., 2017). Considering WetCHARTs treats rice paddies
 275 (main source as AGS) as one wetland type, AGS in EDGAR was excluded and we assume
 276 WetCHARTs represent all wetland CH₄ emissions as natural wetland and rice paddies.

277

278 2.3 Bayesian inversion framework

279 The Scale Factor Bayesian inversion (SFBI) approach was applied to interpret the atmospheric
 280 CH₄ concentration (or enhancement) variations in terms of quantitative constraint on all CH₄
 281 sources. The relationship between observed and simulated CH₄ concentrations (or enhancement)
 282 can be expressed as follows in Equation 1:

$$283 \quad y = \mathbf{K}\Gamma + \varepsilon \quad (1)$$

284 Where y is the observed CH₄ concentration (or enhancement), \mathbf{K} corresponds to simulated
 285 enhancements from all categories, Γ is the state vector to be optimized and consists of *posteriori*
 286 SFs for corresponding categories in \mathbf{K} , and ε is the observing system error.

287

288 The optimal solution to derive *posteriori* SFs is to minimize a cost function $J(\Gamma)$, which represents
 289 the mismatch between CH₄ observations and simulations and the mismatch between *posteriori* and
 290 *a priori* SFs (Miller et al., 2008; Griffis et al., 2017). The cost function $J(\Gamma)$ can be expressed as:

$$291 \quad J(\Gamma) = \frac{1}{2} \left[(y - \mathbf{K}\Gamma)^T S_e^{-1} (y - \mathbf{K}\Gamma) + (\Gamma - \Gamma_a)^T S_a^{-1} (\Gamma - \Gamma_a) \right] \quad (2)$$

292 where S_e and S_a are the constructed error covariance matrices for observations and the *a priori*
 293 values, and S_e consists of measurement and model errors. Here each element in *a priori* SFs Γ_a
 294 is treated as 1. Therefore, the solution for obtaining the *posteriori* SFs is to solve $\nabla_{\Gamma} J(\Gamma) = 0$,
 295 and is given by,

296
$$\Gamma_{\text{post}} = (K^T S_e^{-1} K + S_a^{-1})^{-1} (K^T S_e^{-1} y + S_a^{-1} \Gamma_a)$$
 (3)

297 In the Bayesian inversion framework, we first need to give an estimate of the error covariance
 298 matrices and the state vector for the *a priori* and observational data. And following our previous
 299 studies conducted in East China (Hu et al., 2019; 2022). Uncertainties of 10%, 13% and 20% were
 300 assigned to the measurement errors (S_{obs}), the finite number of particles (500) released in the
 301 STILT model ($S_{\text{particles}}$) and uncertainty in meteorological fields (S_{met}), respectively.

302

303 A previous study derived uncertainties of CH₄ from waste treatment and other categories, which
 304 varied between 30% and 50%, these uncertainties were calculated mainly from activity data and
 305 EFs at the country scale on annual averages (Solazzo et al. 2021). We should also note CH₄
 306 emissions uncertainty will largely increase as the study region size decreases, and, as stated above,
 307 the relative difference among different inventories can reach 150%. Considering the
 308 disaggregation of spatial distributions and temporal variations, CH₄ emission uncertainties can be
 309 much larger at urban and monthly scales. To provide robust constraints on CH₄ emissions in our
 310 study, we used three cases of *a priori* uncertainty combinations for different emissions in Bayesian
 311 inversion:

312 (1) the first case use three elements as wetland, waste treatment and all other anthropogenic
 313 sources, considering the larger seasonality of waste treatment, the uncertainties of 300% was used
 314 for waste treatment and 200% for other categories, (2) the second case have more detailed
 315 categories as wetland, waste treatment, fuel exploitation, energy for building, and the other
 316 anthropogenic sources, where the *a priori* uncertainty of 200% was used for each category, (3) the
 317 third case has the same categories as case 1 but uses a different *a priori* uncertainty for waste
 318 treatment of 200%. The averages of all three cases are used as final *posteriori* SFs and the largest
 319 difference between each of three cases is used as the final uncertainty.

320

321 **3. Results**

322 **3.1 Atmospheric CH₄ observations**

323 We first display the hourly CH₄ concentrations from our three tower-based sites and smoothed
 324 background at five sites by CCGCRV fitting method (Thoning et al., 1989) in Figure 2a. The

325 hourly observations at three towers show similar temporal variations but with different amplitudes.
326 Observations at Hangzhou site vary between 2000 ppb and 2800 ppb, and were much larger than
327 both Linan site and Damingshan site. Their monthly averages are also compared in Figure 2b, and
328 results show the monthly CH₄ vary between lowest 2106.3 ppb in July and highest 2225.0 ppb in
329 September (annual mean of 2159.9 ppb) at Hangzhou site, lowest 2023.3 ppb in July and highest
330 2132.0 ppb in September (annual mean of 2086.7 ppb) at Linan site, the lowest 1955.5 ppb in July
331 and without observations in September at Damingshan site (annual mean of 2013.4±(3) ppb,
332 where the uncertainty was calculated based on the assumption that the values of monthly mean
333 CH₄ concentration in September and October are in between August and November), respectively.
334 The similar trends among the three sites can be explained by all three sites being dominated by
335 similar atmospheric transport processes, such as synoptic process (i.e. monsoon) and seasonally
336 changing wind directions as summarized above. But their surrounding emission sources are highly
337 different, implying the emissions of Hangzhou site should be much larger than Linan and
338 Damingshan sites.

339

340 Because the CH₄ background is important in concentration simulation and emission inversion, we
341 also compare CH₄ background between five sites, where the annual averages at TAP, YON, RYO,
342 WLG and UUM were 1989.8 ppb, 1850.1 ppb, 1982.7 ppb, 1973.4 ppb and 1984.2 ppb,
343 respectively. We found the differences were generally within 20 ppb among TAP, RYO, WLG and
344 UUM sites (Figure 2), but there was large difference between YON site and other four sites from
345 May to August, which can reach to around 100 ppb. Note YON site is located in the south of East
346 China Sea (Figure 1a), it can be influenced by monsoon with clean air flows from the South China
347 Sea, which has many fewer CH₄ sources compared to air flows from East Asia. The CH₄
348 background at TAP site appeared slightly higher than other four sites because TAP site is located
349 on the coast of South Korea and can be more easily polluted by anthropogenic emissions.
350 Considering the large spatial difference between the CH₄ background sites, monthly air flows and
351 source footprint will be used to identify backgrounds for our observation network, with details
352 discussed in Supplementary Material (Section S1, Figure S3 and Table S1).

353

354 **3.2 Concentration footprint and the *a priori* emissions**

355 To illustrate the potential source regions of the three sites, annual averages of simulated footprints
356 for each site are displayed in Figure 3a-c. The results show their footprint distributions were quite
357 similar because of close distance, but we also notice there were obvious differences in the
358 footprint strengths (i.e. the area covered by red color) with Hangzhou site > Linan site >
359 Damingshan site. The reason why the footprint at the Damingshan site is the lowest can be
360 explained by the fact that the observations were collected at 1500 m height, and it was not easy to
361 receive emissions signals within the boundary layer at that height. Besides, the Hangzhou site is
362 located in the core urban area of Hangzhou city, and it will show significant diurnal variation in
363 PBLH, especially since it has higher nighttime PBLH caused by anthropogenic heat and high
364 buildings than grassland/farmland, which dominate Linan site and Damingshan site. Hence more
365 air particles can remain within PBLH and generate stronger footprint.

366

367 The *a priori* EDGAR CH₄ emissions for total anthropogenic categories, waste treatment and its
368 proportions are given in Figure 3d-f. Significant gradients are observed from higher emissions in
369 the east to lower emissions in the west, which is consistent with our three tower-based sets of
370 observations. And the CH₄ emissions for waste treatment indicated similar spatial distributions
371 with urban land use and population density (Figure 1c-d). Moreover, waste treatment seems to
372 emit CH₄ as area sources instead of point sources from waste treatment super plants. Although a
373 few previous studies found limitations of EDGAR inventory to capture CH₄ emission patterns in
374 some urban areas (Pak et al., 2021), here considering the fact that locations of landfills (Figure
375 1b-d), which is the largest anthropogenic CH₄ emitter in Hangzhou city, are very close to the core
376 urban area and in high consistency with EDGAR, hence we believe the spatial patterns of EDGAR
377 in study region to be reliable. We should note the Chinese government constructed waste
378 separation stations in each city with density of one station for per 150~200 households (around
379 450~800 people), usually these waste separation stations are full with waste because domestic
380 garbage can be generated every day, they do not have gas collection systems and can emit large
381 quantity of CH₄ emissions caused by daily biomass waste as area sources (Tian et al., 2022).
382 Besides, there is only one landfill that has gas collection systems, the reported gas collection

383 efficiency was less than 80%, which also indicates large quantity of CH₄ emissions will be directly
384 emitted into the atmosphere and the emissions will be influenced by climate change. These above
385 analyses also imply Hangzhou site can observe higher emissions from both waste treatment and
386 total anthropogenic emissions, which will be discussed and quantified later.

387

388 **3.3 Simulation of CH₄ concentrations and its components for three sites**

389 Comparisons between observed and simulated daily CH₄ concentration averages are displayed in
390 Figure 4a-c and hourly concentrations in Figure S4 for three sites. First, the hourly simulations in
391 Figure S4 show high consistency when only comparing the temporal patterns with observations,
392 indicating good performance of model transport simulations as confirmed in Figure S5 for
393 evaluating meteorological fields. But the relative variations display obvious differences among the
394 three sites for daily averages in Figure 4a-c. The mean bias (MB), root mean squared error
395 (RMSE), and correlation coefficient (R) between daily observations and *a priori* simulations were
396 64.1 ppb, 129.2 ppb and 0.44, respectively, for Hangzhou site; and were -6.0 ppb, 57.1 ppb, 0.50
397 for Linan site, 36.2 ppb, 55.6 ppb, 0.54 for Damingshan site. As for the Hangzhou site, simulated
398 CH₄ concentrations show obvious overestimation from October to April, and the overestimation is
399 also found at Damingshan site. We found that the simulations at the Linan site showed overall
400 good agreement with observation, but still with slight overestimation from January to April and
401 underestimation from May to September. Considering the source area contributions for the three
402 sites are different, these differences among the three sites indicated the bias in CH₄ emission
403 largely varied from Hangzhou city to larger regional scale.

404

405 To further quantify detailed contributions from different regions and categories to each tower site,
406 CH₄ enhancements from different categories and source areas were also simulated separately for
407 the three sites. As displayed in Figure 4d-e, the simulated *a priori* total enhancements at Hangzhou
408 site, Linan site, and Damingshan site were 244.3 ppb, 100.8, and 69.0 ppb, respectively. We also
409 found contributions by waste treatments dominated the total enhancements but with obvious
410 differences among the three sites, which varied from the highest 64.2% at Hangzhou site to the
411 lowest 41.4% at Damingshan site. We further calculated anthropogenic contributions from

412 Hangzhou city (excluding wetlands because of coarser spatial resolution for Hangzhou city) and
413 other provinces, which were 158.4 ppb at Hangzhou site, 30.7 ppb at Linan site, and 10.1 ppb at
414 Damingshan site, respectively. And they accounted for 69.3%, 34.0%, and 16.9% of total
415 anthropogenic enhancements at corresponding sites. These results indicate the CH₄ observations at
416 Hangzhou site, which is located at the core urban region, are more influenced by local emissions
417 (mainly for waste treatment which will be discussed later) and contain much higher enhancements
418 than the other two sites. The relative contributions from Hangzhou city to observations at the
419 Hangzhou site, Linan site and Damingshan site were 158.4 ppb (69.3% to total CH₄ enhancement),
420 30.7 ppb (34.0% to total CH₄ enhancement), and 10.1 ppb (16.9% total CH₄ enhancement),
421 respectively. The relative contributions from Zhejiang province to observations at the Hangzhou
422 site, Linan site and Damingshan site were 181.7 ppb (79.5% to total CH₄ enhancement), 44.3 ppb
423 (49.0% to total CH₄ enhancement), and 17.9 ppb (29.9% total CH₄ enhancement), respectively.
424 These different values also imply that the observations at Linan and Damingshan sites can
425 represent CH₄ emissions of much larger region as Zhejiang province or YRD area than Hangzhou
426 city (Figure 4e), and Damingshan site.

427

428 The seasonally averaged diurnal variations for both observations and simulations are also
429 displayed in Figure 5 for the three sites. Although many previous studies only used daytime
430 observations and simulations to evaluate *a priori* emissions bias and constrain emissions (Sargent
431 et al., 2018; Hu et al., 2022), these studies were based on the assumption that the diurnal scaling
432 factors used for the *a priori* emissions are right (i.e. for anthropogenic CO₂), or the emissions do
433 not have obvious diurnal variations (i.e. emissions from industries or manufacturing). As
434 concluded above, the main CH₄ component in Hangzhou city was waste treatment (Figure 3f),
435 which should be highly sensitive to temperature and indicates obvious diurnal and seasonal
436 patterns (Mønster et al., 2019; Kumar et al., 2022). And total CH₄ emissions will be overestimated
437 when using daytime emissions to represent all-day averages. Further, we found strong similarities
438 of the diurnal variations between observations and simulations for the three sites, but there are still
439 some discrepancies especially that the observations at Linan site were generally higher than
440 simulations from spring to autumn for both all-day and midday averages.

441 Hence, our preliminary conclusions were that the *a priori* CH₄ emissions were generally
442 overestimated for Hangzhou city but underestimated in the larger region of Zhejiang or YRD area.
443 We also found simulations were higher than observations for all seasons at Damingshan site, and it
444 can be explained by the complex topography around the Damingshan site, where elevations
445 changed from 0 m to 1600 m within the site's grid cell of 9 km (~ 0.1°) as displayed in Figure 1b,
446 and the mountain-valley wind patterns, PBLH changes can only be resolved with much higher
447 spatial resolutions of < 1km. Hence the use of coarse resolutions (i.e. 9 km in this study) at the
448 mountainous regions introduces large bias in simulating concentration and emission inversion, as
449 also recently found in China for CO₂ as “aggregation error” (Agustí-Panareda et al., 2019; Wang et
450 al., 2022), so observations at Damingshan site will not be used in emissions inversions in this
451 study.

452

453 **3.4 Constraints on anthropogenic CH₄ emissions**

454 As displayed in Figures 3f, 5a and concluded in Section 3.3, simulations using *a priori* CH₄
455 emissions show obvious overestimation especially from October to April at Hangzhou site, and
456 emissions were also overestimated in winter and underestimated from spring to autumn at Linan
457 site. Note this bias can be attributed to *a priori* emissions or meteorological simulations. Our
458 previous studies in YRD have evaluated the meteorological simulations by using the same
459 physical parameterization schemes, which showed high consistency with observations (Hu et al.,
460 2019; 2021; 2022; Huang et al., 2021). We also evaluated the meteorological simulations with
461 observations and confirmed the good model performance (Figure S5). Note that PBLH
462 simulations are important in evaluating model performance. However, we only have four months
463 of hourly PBLH observations, one month in each season. These hourly PBLH observations were
464 used to evaluate the general performance of WRF model. As displayed in Figure S6, it shows
465 overall good performance for both daytime and nighttime PBLH variations. Furthermore, we
466 found no monthly variations in EDGAR v6.0 CH₄ emissions for waste treatment, which
467 contributed 64.2% to annual CH₄ enhancement average and much higher in winter (Figure S7-S8).
468 The CH₄ emissions from waste treatment are produced by the microbial process, which should be
469 affected by meteorological conditions especially by seasonal temperature changes. Hence our

470 assumption is that the bias in both its seasonality and annual average lead to large
471 overestimation/underestimation in the simulated CH₄ concentration. Besides, bias in other
472 anthropogenic emissions and wetlands can also partly contribute to the bias of the simulated CH₄
473 concentration.

474

475 To quantify the bias sources and constrain corresponding *a priori* emissions for Hangzhou city, we
476 applied the scaling factor Bayesian inversion approach with three different cases as introduced in
477 the Method section. Instead of only using daytime CH₄ observations to constrain *a priori*
478 emissions, we choose to use all-day hourly data at Hangzhou site to constrain emissions for
479 Hangzhou city, for the following three reasons: (1) the enhancements contributed by Hangzhou
480 city at the Hangzhou site was 69.3%, and much larger than 34.0%, and 16.9% for Linan site and
481 Damingshan site, respectively; (2) the waste treatment dominated anthropogenic CH₄ emissions in
482 Hangzhou city, which is caused by biological process and should be temperature dependent. Since
483 the observed temperature varied diurnally by 20 °C, the use of only daytime observations without
484 considering diurnal CH₄ emissions will bring significant bias when using derived daytime
485 emissions to represent all-day averages. The annual averages of daytime and all-day average
486 concentrations were 2112.4 and 2156.0 ppb at Hangzhou site, respectively, the reason why higher
487 emissions in daytime correspond to lower concentration than in all-day and nighttime is that lower
488 PBLH in nighttime will lead to higher concentration, and more comparisons between daytime and
489 all-day average concentrations are displayed in Figure 5 for three sites; (3) previous studies using
490 daytime observations were mainly conducted for regions dominated by industry or energy
491 production, which have much smaller diurnal variations than waste treatment as stated above
492 (Mønster et al., 2019; Kumar et al., 2022).

493

494 The derived monthly *posteriori* SFs for each emission source are displayed in Table 1 for
495 Hangzhou city. The results show that the *posteriori* SFs for waste treatment are much smaller in
496 winter and higher in summer, indicating obvious seasonality and the overestimation in winter was
497 mainly contributed by waste treatment. The annual mean *posteriori* SFs for waste treatment vary
498 between 0.50 and 0.56 in all three cases, illustrating overestimation at annual average for the *a*

499 *priori* waste treatment emissions. Besides, the annual mean *posteriori* SFs vary between 0.87 and
500 0.94 for the rest of the total anthropogenic categories (excluding agricultural soil), and are 0.97 for
501 PRO (fuel exploitation) and 0.91 for RCO (energy for building), respectively; the annual mean
502 *posteriori* SF is 1.05 for wetland (including agricultural soil and natural wetland). These *posteriori*
503 SFs for the rest anthropogenic categories and wetland indicate much smaller bias than waste
504 treatment. The monthly *posteriori* SFs for PRO and RCO also illustrate obvious seasonal
505 variations, but are still smaller than the *a priori* seasonality in the inventory (Figure S9). Although
506 the evaluations of hourly PBLH simulations have illustrated good performance in both daytime
507 and nighttime (Figure S6), we also conducted inversions by only using daytime observations to
508 constrain CH₄ emissions. Considering results from Case 2 are in between Case 1 and Case 3, here
509 we only display the results from Case 1 and Case 3 (Table S2), it shows similar seasonal variations
510 as using all all-day observations. We notice the values are larger than latter, which is reasonable
511 because CH₄ emissions in daytime should be larger than all-day and nighttime emissions. In
512 general, *posteriori* SFs by using all-day concentration observations will be used to represent total
513 CH₄ emissions from monthly to annual scales.

514

515 To evaluate whether the *posteriori* SFs have significantly improved CH₄ emissions, we used these
516 SFs to derive the *posteriori* emissions and re-simulated hourly concentrations in Figure 6 (and
517 daily averages in Figure S9). Results show the hourly overestimation by using *a priori* emissions
518 is largely reduced by using *posteriori* emissions when compared with observations in Figure 6a-b,
519 and the regression slopes between daily averaged observations and simulations decrease from
520 1.51(±0.15) for *a priori* simulations to 0.85(±0.07) for *posteriori* simulations in Figure 6c. The
521 mean bias (MB), root mean squared errors (RMSE), correlation coefficient (R) between daily
522 observations and *a priori* simulations are 64.1 ppb, 129.2 ppb and 0.44, respectively, and these
523 statistics change to -22.2 ppb, 72.3 ppb and 0.58 for *posteriori* simulations. These results indicate
524 the *posteriori* SFs obviously decrease the bias in *a priori* emissions and are closer to observations,
525 when considering there are no system biases in simulated monthly PBLH.

526

527 The comparisons of monthly CH₄ emissions between *a priori* and *posteriori* waste treatment and

528 other anthropogenic sources (excluding agricultural soil) in Hangzhou city are displayed in
529 Figures 7a and S7. For the *a priori* inventory, there is not seasonal variations for waste treatment
530 with constant monthly emissions of 8.67×10^3 t, and other anthropogenic sources show
531 seasonality with much higher in winter (i.e. 5.22×10^3 t in January) than in summer (i.e. $3.06 \times$
532 10^3 t in August). The seasonality in *a priori* EDGAR inventory is mainly dominated by RCO
533 (Energy for buildings), with proportions to total anthropogenic emissions changing from the
534 highest 22% in winter to lowest 8% in summer. Such information indicates the *a priori* inventory
535 assigned more leaks from natural gas distribution infrastructure in winter than in summer. As
536 discussed above, constant emissions from waste treatment should be wrong because of its large
537 temperature sensitivity, and the observed monthly temperature difference between summer and
538 winter was larger than 25°C in Hangzhou city in study period. After including the constraints from
539 the observed concentrations, the *posteriori* emissions for waste treatment show obvious
540 seasonality with highest emission in July ($7.66 \pm 0.09 \times 10^3$ t) and lowest emission in February
541 ($2.20 \pm 0.87 \times 10^3$ t). And emissions from other anthropogenic categories show much smaller
542 seasonality (highest emission in January of $4.18 \pm 0.69 \times 10^3$ t and lowest emission in August of
543 $2.88 \pm 0.15 \times 10^3$ t) than *a priori* emissions. In general, the annual emissions from waste treatment
544 were 10.4×10^4 t in the *a priori* EDGAR inventory and decreased to $5.5 (\pm 0.6) \times 10^4$ t for the
545 *posteriori* emissions, a decrease of 47.1%. The *a priori* emissions from other anthropogenic
546 sources were 4.5×10^4 t and only slightly decreases to $4.1 (\pm 0.3) \times 10^4$ t for the *posteriori*
547 emissions, an 8.9% decrease. The proportion of waste treatment to total anthropogenic emissions
548 decreases from *a priori* 69.3% to *posteriori* 57.3%. To summarize, the annual total anthropogenic
549 CH₄ emission (excluding agricultural soil) decreases from 15.0×10^4 t to $9.6 (\pm 0.9) \times 10^4$ t,
550 indicating overestimation of 36.0% in Hangzhou city for the *a priori* emissions.

551

552 However, as concluded above the observations and simulations at Linan site, which represents the
553 much larger region of Zhejiang province or YRD area, data from that site indicated slightly
554 different results that CH₄ simulations were underestimated from spring to autumn and
555 overestimated in winter (Figure 4b and Figure 5e-h). Here we used the multiplicative scaling
556 factor (MSF) method and observations at Linan site to derive SFs at seasonal scale (Sargent et al.,

557 2018; He et al., 2020), where we used 10 ppb as the potential CH₄ background uncertainty in
558 winter, spring and autumn, and 20 ppb in summer, see details in the Supplementary Material
559 (Section S2). The derived *posteriori* SFs were 0.87 (± 0.08), 1.07 (± 0.11), 1.19 (± 0.24), and 1.16
560 (± 0.11) for winter, spring, summer, and autumn, respectively. The results for the Linan site
561 showed similar seasonal variations as found for Hangzhou city and was 1.07 (± 0.14) of *a priori*
562 anthropogenic emissions for the annual average. Our observations at Hangzhou site and Linan site
563 together indicate the *a priori* emissions were largely biased on both seasonal and annual scales,
564 and the annual anthropogenic CH₄ emission was largely overestimated by 36.0% in Hangzhou city,
565 but was underestimated by 7.0% in the larger region of Zhejiang province or YRD area.

566

567 **3.5 Temperature sensitivity of waste treatment CH₄ EFs and projected changes**

568 Although the derived *posteriori* monthly SFs on waste treatment reflected changes on emissions,
569 considering the monthly activity data does not have obvious monthly changes, these SFs can
570 mainly reflect relative variations of monthly EFs and contain meteorological dominated changes
571 especially for temperature. To evaluate the temperature sensitivity of its EFs, we first calculated
572 the normalized monthly SFs by dividing monthly SFs by annual averages (Tables 1 and S3), and
573 quantified the relationship between observed T_{2m} and normalized SFs. Note decomposition of
574 organic waste by methanogens mostly takes places at some depth within the landfills and
575 temperature can be higher than at the surface, hence the temperature within landfills should be
576 much more related to methanogens activities and CH₄ emissions than T_{2m}. However, considering
577 (1) we do not have direct temperature observations under landfills, (2) T_{2m} can be used as indicator
578 of methanogens activities, and (3) T_{2m} is commonly used meteorological data that can be provided
579 for future RCP scenarios, hence the relationship between waste CH₄ emissions and T_{2m} is
580 constructed and used to predict how will CH₄ EFs change in different climate scenarios. The
581 normalized SFs illustrate significant linear relationship with monthly T_{2m} (Figure 7b), where the
582 slopes imply that normalized SFs (and EFs) will increase by 38%~50% with temperature increase
583 by 10°C at city scale. We also analyzed the temperature sensitivity by only using daytime CH₄
584 observations and simulations in Figure S10, it still shows strong linear relationship between
585 normalized SFs and T_{2m}, with the slopes of 0.046 and 0.060. These results are in high consistency

586 with using all-day observations of 0.038 and 0.050, indicating similar results of using 24 hours
587 observations and only using daytime observations, and less influence of simulated nighttime
588 PBLH bias on corresponding temperature sensitivity.

589

590 We should note the precipitation, soil water content and atmospheric pressure can also have
591 obvious influence on CH₄ emissions, and considering the fact that we have not conducted field
592 measurement in landfills and landfills are usually covered by metal or plastic in China to avoid the
593 spread of odors, hence reanalysis data cannot represent real soil water contents in these site scale
594 landfills. Precipitation and atmospheric pressure show obvious linear relationship with
595 temperature as displayed in Figure S11. They display positive linear relationship between
596 precipitation (affect water content) and T_{2m}, and negative linear relationship between monthly
597 averaged atmospheric pressure and T_{2m}. We also found negative relationship between atmospheric
598 pressure and normalized SFs, and positive relationship between T_{2m} and normalized SFs (Figures
599 7b and S11). Considering air temperature always displays negative relationship with atmospheric
600 pressure as warmer air temperature coincides with lighter air mass and lower atmospheric pressure
601 in summer as displayed in Figure 11b, and colder air temperature coincides with heavier air mass
602 and higher atmospheric pressure in winter. Hence, the temperature can be used to represent
603 co-influence of both temperature and atmospheric pressure, and we only focus on the influence of
604 temperature on CH₄ emissions and will add more supporting data in following studies.

605

606 Our findings for the high sensitivity of waste treatment CH₄ emissions to temperature also suggest
607 a dramatic increase with the projection of future global warming trends. We further derived the
608 T_{2m} trends for four different RCP scenarios as RCP8.0, RCP6.0, RCP4.5 and RCP2.6 (Figure 8a).
609 The results show T_{2m} will increase by 0.50°C, 0.28°C, 0.16°C, 0.10°C per decade for Hangzhou
610 city, respectively. These different warming trends also indicate distinct temperature-dominated
611 influence on future CH₄ EFs and emissions from waste treatment. We then used the slopes from
612 Figure 7b and annual temperature from 2021 to 2100 to derive relative changes of EFs in future 80
613 years, where observations for year 2021 were treated as the baseline year. As displayed in Figure
614 8b, the EFs in RCP8.5, RCP6.0, RCP4.5 and RCP2.6 scenarios will increase with the rates of

615 2.2%, 1.2%, 0.7% and 0.5% per decade, respectively. And CH₄ EFs for waste treatment will be
616 higher by 17.6%, 9.6%, 5.6%, and 4.0% at the end of this century.

617

618 The spatial distribution of T_{2m} trends for all of China is also displayed in Figure S12, which shows
619 heterogeneous distribution across China for four global warming scenarios. Because East China
620 has high population density, with the majority of the national population (Figure S1), and is
621 responsible for the largest domestic garbage induced CH₄ emissions (Figure S2), these combined
622 factors indicate considerable CH₄ emissions changes from waste treatment in such a
623 temperature-sensitivity area. Considering that the temperature sensitivity of waste treatment CH₄
624 EFs is caused by microbial process at regional scales, the sensitivity can represent general
625 conditions of different cities or landfills. And if we assume the derived temperature sensitivity
626 (increase by 44% with temperature increases of 10°C on average) is applicable for China as a
627 whole, especially for East China, the relative changes of waste treatment CH₄ EFs can be
628 calculated by multiplying this value by air temperature trends. The spatial distribution of global
629 warming induced EF changes at the end of this century is displayed Figure 9. For RCP2.6 scenario,
630 EFs for waste treatment will slightly increase by 4.0-6.5% in the north eastern China and increase
631 by 3.0-4.0% in south eastern China. The RCP6.0 also displayed heterogeneous changes in East
632 China, with EFs in the north eastern China increasing by 10.5-13.0% and in south eastern China
633 increasing by 9.0-10.5%. Relative changes in RCP4.5 and RCP8.5 are more homogeneous for East
634 China, which indicates EFs will significantly increase by 5.0-7.5% and 17.5-19.5%, respectively.
635 The largest changes will occur in West China for RCP8.5, with EFs increasing by >20.0%, but this
636 area has low population density and CH₄ emissions, and therefore these effects of global warming
637 can be ignored (Figure S12). Finally, we should note these derived relative changes are only
638 caused by global warming, and the influence of activity data, management technology and other
639 factors is not considered and out of the scope of this study.

640

641 **4 Discussions and implications**

642 Many previous studies have compared total CH₄ emissions and its components for different
643 inventories and bottom-up methods, which illustrated large uncertainty and bias at city scale and

644 these biases were much larger for waste treatment (Peng et al., 2016; Saunois et al., 2020; Lin et
645 al., 2021; Bian et al., 2022). A recent bottom-up research compared wastewater CH₄ EFs in China,
646 which largely varied by four-fold in different provinces and the uncertainty in the same province
647 were even two-fold larger than its average, implying considerable uncertainty in recent
648 understanding of waste treatment EFs at regional scale (Hua et al., 2022). And for the national
649 total emissions, waste treatment CH₄ emissions varied between 5 and 15 Tg a⁻¹ (Peng et al., 2016;
650 EDGAR v6). There are also other atmospheric inversion studies in estimating China's CH₄
651 emissions (Hopkins et al., 2016; Hu et al., 2019; Huang et al., 2021; Miller et al., 2019; Lu et al.,
652 2021; Chen et al., 2022). These studies found large variations of national emissions for almost all
653 inventories, which were mainly caused by fossil fuel exploitation, agricultural sector (livestock
654 and rice paddies) and waste treatment. For the comparisons of waste treatment emissions, these
655 satellite-based inversions also largely varied between 6 and 9 Tg a⁻¹ by 1.5-fold (Miller et al.,
656 2019; Lu et al., 2021; Chen et al., 2022; Zhang et al., 2022).

657

658 The reported discrepancies between “bottom-up” and “top-down” approaches indicate large
659 uncertainty in understanding China's national CH₄ emissions from waste treatment. And it is well
660 known the uncertainties will increase from national scale to regional and city scales, also implying
661 considerable uncertainties in city-scale emissions for inventories. But the atmospheric inversion
662 approach for city scale waste treatment, which can act as an independent evaluation, is still rare
663 not only for China but also globally. To our best knowledge, there is only one recent atmospheric
664 inversion research focused on CH₄ emissions from city-scale waste treatment, which used
665 satellite-based observation to constrain emissions from four cities in India and Pakistan, that
666 concluded underestimation of landfills CH₄ emissions by 1.4 to 2.6 times for EDGAR inventory
667 (Maasackers et al., 2022). In our study, we found annual waste CH₄ emissions were overestimated
668 by 47.1% for Hangzhou city, our findings are different from results in India and Pakistan. These
669 differences indicate bias of waste treatment CH₄ emissions considerably varied in different
670 countries and climate divisions. Our results highlight there is a large knowledge gap in
671 understanding waste treatment emissions mechanisms and estimating urban waste treatment CH₄
672 emissions especially in China.

673 Different from fossil-type sources that have much smaller monthly variations, CH₄ emission from
674 waste treatment is biological processes-based source and its EFs are highly sensitive to
675 meteorological conditions especially for temperature. These factors lead to obvious bias in waste
676 treatment CH₄ emissions not only for annual average but also for its seasonality. Besides, although
677 there were a few studies that aimed to predict future CH₄ emissions from waste treatment, these
678 studies were mainly based on activity data changes without considering the EFs variations caused
679 by future global warming trends or only based on site-specific observations (USEPA 2013; Cai et
680 al., 2018; Spokas et al., 2021). Of these three cited studies, USEPA (2013) and Cai et al. (2018)
681 only predicted emissions changes due to changes in activity data and management technology.
682 And the CH₄ emissions for year 2030 by Cai et al. (2018) was 23.5% lower than the USEPA
683 (2013) estimation, which was caused by the consideration of new policies and low-carbon policy
684 scenarios. Spokas et al. (2021) modeled the CH₄ emission changes with increasing air
685 temperature, where CH₄ emissions did not show obvious changes even with temperature
686 increasing by ~5°C by the end of year 2100. To our best knowledge, there are no inventories that
687 considered the temperature-induced changes on both seasonal variations and annual trends of CH₄
688 emissions. Hence, it is still unclear in all inventories how EFs will change with different global
689 warming scenarios at city scale.

690

691 A few observation-based measurements were conducted for waste treatment but only at some
692 specific sites with large discrepancies of EFs (Du et al., 2017; 2018; Cai et al., 2018; Zhao et al.,
693 2019; NBSC, 2015; Wang et al., 2015; Florentino et al., 2010; Tolaymat et al., 2010; Cai et al.,
694 2014; 2018). And only one of our previous studies used year-round atmospheric CH₄ observations
695 to constrain regional scale CH₄ emissions at Nanjing city in YRD area (Huang et al., 2021), where
696 it found much higher emissions of the landfilling waste in summer than in winter: CH₄ emissions
697 in July were around four times those in February. But there is no study that has quantified the
698 temperature sensitivity of waste CH₄ emissions at city scale or much larger regional scales. These
699 two studies in different cities confirmed temperature as the dominant factor that drives seasonal
700 variations of waste treatment CH₄ emissions. Hence our study appears as the first one that
701 estimated city scale waste treatment CH₄ emissions, its temperature sensitivity and projected

702 changes in different global warming scenarios. Our findings for the large sensitivity to
703 temperature indicate the monthly scaling factors should be considered to better represent CH₄
704 emissions and simulate atmospheric CH₄ concentrations.

705

706 We also note that the predictions of future climate changes are mainly based on different emitting
707 intensity of greenhouse gas, and CH₄ contributed around 20% of direct anthropogenic radiative
708 forcing (Seto et al., 2014). The CH₄ emissions in different global warming scenarios were mainly
709 calculated by predicting energy use data without considering the changes of EFs. In this study, we
710 found there should be large positive feedback between global warming and CH₄ emissions,
711 especially in the RCP 8.0 scenario where global warming induced CH₄ emissions from waste
712 treatment will increase by 17.6%. Hence the projected emissions from waste treatments and other
713 biological process based sources, together with positive feedback between temperature and their
714 emissions are strongly suggested in future climate change models. Besides, it is well known that
715 CH₄ concentration simulations are essential for modeling air pollutions (e.g. O₃, NO_x, and CO)
716 especially in the stratosphere (Isaksen et al., 2011; Kaiho et al., 2013). Considering that waste
717 treatment CH₄ emissions accounted for ~25% of total anthropogenic emissions (EDGAR v6.0) in
718 East China where severe air pollution frequently occurred, we also believe the coupling of
719 temperature-dependent CH₄ emissions and the monthly scaling factors on CH₄ emissions can
720 improve air pollution modeling in East China.

721

722 We should note that new technology and other meteorological variables can also influence waste
723 treatment CH₄ emissions. The main reason to only use temperature in this study is that we only
724 constrained the emissions at monthly scale in one year, and derived twelve datasets of *posteriori*
725 CH₄ emissions. Besides, temperature is considered to be the main factor in controlling monthly
726 and annual variations of waste treatment CH₄ emissions, and can be used to represent the
727 co-influence of other meteorological parameters such as atmospheric pressure. We will use
728 multiple years' CH₄ concentration to quantify the influence of new technology and other
729 meteorological variables on waste treatment CH₄ emissions in our following study, and we suggest
730 that other tracers (e.g. ethane, ¹⁴CH₄) are also important to separate CH₄ emissions from biological

731 and fossil CH₄ emissions.

732

733 **5 Summary and Conclusions**

734 To better evaluate bias for city scale anthropogenic CH₄ emissions and understand the sensitivity
735 of temperature on waste treatment CH₄ emissions, we used a three tower-based atmospheric CH₄
736 observation network in Hangzhou city, which is located in the developed YRD region and one of
737 the top 10 megacities in China. One-year hourly atmospheric CH₄ observations were presented
738 from December 2020 to November 2021. We then applied a scaling factor Bayesian inversion
739 method to constrain monthly anthropogenic CH₄ emissions and its components (especially for
740 waste treatments) in Hangzhou city, and also used multiplicative scaling factor method for broader
741 Zhejiang province and YRD area at seasonal scale.

742

743 To the best of our knowledge, our study is the first tower-based CH₄ observation network in China.
744 We found obvious seasonal bias of simulated CH₄ concentrations at the core urban area of
745 Hangzhou city, which was mainly caused by bias of waste treatment at both annual and monthly
746 scales. The derived *posteriori* CH₄ emissions display obvious seasonal variations with peak in
747 summer and trough in winter, which was mainly contributed by waste treatment; the *a priori*
748 annual waste treatment CH₄ emission in Hangzhou city was 10.4×10^4 t and decreased to 5.5
749 $(\pm 0.6) \times 10^4$ t for the *posteriori* emissions, a decrease of 47.1%. Besides, the total anthropogenic
750 CH₄ emissions (excluding agricultural soil) decreased from 15.0×10^4 t to $9.6(\pm 0.9) \times 10^4$ t,
751 indicating overestimation of 36.0% for the whole year of 2021. Observations at Linan site imply
752 that the annual CH₄ emissions was slightly underestimated by 7.0% for the larger region of
753 Zhejiang province or YRD area, which was different from the case of Hangzhou city. Additionally,
754 the *posteriori* monthly CH₄ emissions from waste treatment illustrate significant linear
755 relationship with air temperature, with regression slopes indicating an increase of 38%~50% when
756 temperature increases by 10°C. Finally, we found the waste treatment CH₄ EFs for Hangzhou city
757 will increase by 17.6%, 9.6%, 5.6%, and 4.0% by the end of this century for RCP8.0, RCP6.0,
758 RCP4.5 and RCP2.6 scenarios, respectively. The derived relative changes for whole China also
759 showed high heterogeneity and indicate large uncertainty in projecting future national total CH₄

760 emissions. This study is also the first one that mainly focuses on city scale temperature sensitivity
761 of waste treatment CH₄ emissions from the perspective of atmospheric inversion approach. And
762 based on above results, we strongly suggest the temperature-dependent EFs should be coupled in
763 both recent CH₄ inventories and future CH₄ emission projections.

764

765 **Data availability:** The atmospheric CH₄ observations data can be requested from Cheng Hu and
766 Bing Qi. STILT model is downloaded from <http://www.stilt-model.org/>, the EDGAR inventory is
767 from <https://edgar.jrc.ec.europa.eu/>, and the projected climate data were downloaded from World
768 Data Center for Climate (WDCC, <https://www.wdc-climate.de/ui/>).

769

770 **Acknowledgement:** Cheng Hu is supported by the National Natural Science foundation of China
771 (grant no. 42105117) and Natural Science Foundation of Jiangsu Province (grant no. BK20200802).
772 Wei Xiao is supported by the National Key R&D Program of China (grants 2020YFA0607501 &
773 2019YFA0607202). This work is also supported by Zhejiang Provincial Basic Public Welfare Research
774 Project (LGF22D050004). We sincerely thank the detailed comments from two anonymous reviewers.
775 We also want to express our thanks to Prof. Timothy J. Griffis from University of Minnesota, who
776 provided many important suggestions and support for this study.

777

778 **Author contribution:** Cheng Hu and Bing Qi designed the study. Cheng Hu performed the model
779 simulation, data analysis and wrote and revised the paper; Bing Qi and Rongguang Du conducted CH₄
780 concentration observation and meteorological data collection, and all co-authors contributed to the
781 data/figures preparation and analysis.

782 **Declaration of competing interests:** The authors declare that they have no conflict of interest.

783

784 **References:**

785 Agustí-Panareda, A., Diamantakis, M., Massart, S., Chevallier, F., Muñoz-Sabater, J., Barré, J., Curcoll, R.,
786 Engelen, R., Langerock, B., Law, R. M., Loh, Z., Morguí, J. A., Parrington, M., Peuch, V.-H., Ramonet, M., Roehl,
787 C., Vermeulen, A. T., Warneke, T., and Wunch, D.: Modelling CO₂ weather – why horizontal resolution matters,
788 *Atmos. Chem. Phys.*, 19, 7347–7376, <https://doi.org/10.5194/acp-19-7347-2019>, 2019.

789

790 Bian R., Zhang T., Zhao F., et al. Greenhouse gas emissions from waste sectors in China during 2006–2019:
791 Implications for carbon mitigation. *Process. Saf. Environ.*, 161:488-497, 2022.

792

793 Bloom, A. A., Bowman, K. W., Lee, M., Turner, A. J., Schroeder, R., Worden, J. R., Weidner, R., McDonald, K. C.,
794 and Jacob, D. J.: A global wetland methane emissions and uncertainty dataset for atmospheric chemical transport
795 models (WetCHARTs version 1.0), *Geosci. Model Dev.*, 10, 2141–2156,
796 <https://doi.org/10.5194/gmd-10-2141-2017>, 2017.

797 Börjesson G, Svensson BH. Seasonal and Diurnal Methane Emissions From a Landfill and Their Regulation By
798 Methane Oxidation. *Waste Management & Research*. 1997;15(1):33-54. doi:10.1177/0734242X9701500104
799

800 Cai, B., J. Liu, X. Zeng, D. Cao, L. Liu, Y. Zhou, Z. Zhang, Estimation of CH₄ emission from landfill in China
801 based on point emission sources. *Adv. Clim. Change Res.* 5, 81–91, 2014.
802

803 Cai, B., Lou, Z., Wang, J., Geng, Y., Sarkis, J., Liu, J., and Gao, Q.: CH₄ mitigation potentials from China landfills
804 and related environmental co-benefits, *Sci. Adv.*, 4, eaar8400, <https://doi.org/10.1126/sciadv.aar8400>, 2018.
805

806 Chen, Z., Jacob, D. J., Nesser, H., Sulprizio, M. P., Lorente, A., Varon, D. J., Lu, X., Shen, L., Qu, Z., Penn, E., and
807 Yu, X.: Methane emissions from China: a high-resolution inversion of TROPOMI satellite observations, *Atmos.*
808 *Chem. Phys.*, 22, 10809–10826, <https://doi.org/10.5194/acp-22-10809-2022>, 2022.
809

810 Du, M., Peng, C., Wang, X., Chen, H., Wang, M., and Zhu, Q.: Quantification of methane emissions from
811 municipal solid waste landfills in China during the past decade, *Renew. Sust. Energ. Rev.*, 78, 272–279, 2017.
812

813 Du, M., Zhu, Q., Wang, X., Li, P., Yang, B., Chen, H., Wang, M., Zhou, X., and Peng, C.: Estimates and
814 predictions of methane emissions from wastewater in China from 2000 to 2020, *Earths Future*, 6, 252–263, 2018.
815

816 Fang S.X., R.G. Du, B. Qi. et al., Variation of carbon dioxide mole fraction at a typical urban area in the Yangtze
817 River Delta, China. *Atmos. Res*, 265, 105884, 2022.

818

819 Florentino, Cruz., B. De La , and M. A. Barlaz ., Estimation of waste component-specific landfill decay rates using
820 laboratory-scale decomposition data. *Environ. Sci. Technol.* 44, 4722–4728, 2010.
821

822 Griffis, T. J., Chen, Z., Baker, J. M., Wood, J. D., Millet, D. B., Lee, X., et al., Nitrous oxide emissions are
823 enhanced in a warmer and wetter world. *P. Natl. Acad. Sci. USA*, 114(45), 12081–12085.
824 <https://doi.org/10.1073/pnas.1704552114>, 2017.

825 He, J., Naik, V., Horowitz, L. W., Dlugokencky, E., and Thoning, K.: Investigation of the global methane budget
826 over 1980–2017 using GFDL-AM4.1, *Atmos. Chem. Phys.*, 2020, 20, 805–827,
827 <https://doi.org/10.5194/acp-20-805-2020>.
828

829 Henne, S., Brunner, D., Oney, B., Leuenberger, M., Eugster, W., Bamberger, I., Meinhardt, F., Steinbacher, M., and
830 Emmenegger, L.: Validation of the Swiss methane emission inventory by atmospheric observations and inverse
831 modelling, *Atmos. Chem. Phys.*, 16, 3683–3710, <https://doi.org/10.5194/acp-16-3683-2016>, 2016.
832

833 Hopkins, F. M., Kort, E. A., Bush, S. E., Ehleringer, J. R., Lai, C.-T., Blake, D. R., & Randerson, J. T. Spatial
834 patterns and source attribution of urban methane in the Los Angeles Basin. *J. Geophys. Res-Atmos.*, 121, 2490–
835 2507, 2016.
836

837 Höglund-Isaksson, L.: Global anthropogenic methane emissions 2005–2030: technical mitigation potentials and
838 costs, *Atmos. Chem. Phys.*, 12, 9079–9096, <https://doi.org/10.5194/acp-12-9079-2012>, 2012.
839

840 Hua, H., Jiang, S., Yuan, Z., Liu, X., Zhang, Y., & Cai, Z. Advancing greenhouse gas emission factors for
841 municipal wastewater treatment plants in China. *Environ. Pollut.*, 295, 118648.
842 <https://doi.org/10.1016/j.envpol.2021.118648>, 2022.

843

844 Hu C, Griffis, T. J., Liu, S., Xiao, W., Hu, N., Huang, W., Yang, D., Lee, X., Anthropogenic methane emission and
845 its partitioning for the Yangtze River Delta region of China. *J. Geophys. Res-Biogeophys.*, 124(5): 1148-1170, 2019.

846

847 Hu, C., Xu, J., Liu, C., Chen, Y., Yang, D., Huang, W., Deng, L., Liu, S., Griffis, T. J., and Lee, X.: Anthropogenic
848 and natural controls on atmospheric $\delta^{13}\text{C}$ -CO₂ variations in the Yangtze River delta: insights from a carbon
849 isotope modeling framework, *Atmos. Chem. Phys.*, 21, 10015–10037, <https://doi.org/10.5194/acp-21-10015-2021>,
850 2021.

851

852 Hu, C., Griffis, T.J., Xia, L., Xiao, W., Liu, C., Xiao, Q., Huang, X., Yang, Y., Zhang, L., Hou, B., Anthropogenic
853 CO₂ emission reduction during the COVID-19 pandemic in Nanchang City, China, *Environ. Pollut.*, 309, 119767,
854 doi: <https://doi.org/10.1016/j.envpol.2022.119767>, 2022.

855 Huang, W. J., T. J. Griffis, C. Hu, W. Xiao, and X. H. Lee. Seasonal variations of CH₄ emissions in the
856 Yangtze River Delta region of China are driven by agricultural activities. *Adv. Atmos. Sci.*, 38(9), 1537–1551,
857 <https://doi.org/10.1007/s00376-021-0383-9>, 2021.

858

859 Isaksen I S, Gauss M, Myhre G, Anthony W, Katey M and Ruppel C 2011 Strong atmospheric chemistry feedback
860 to climate warming from Arctic methane emissions. *Global Biogeochem. Cy.* 25 GB2002, 2011.

861

862 Kumar, P.; Broquet, G.; Caldow, C.; et al. Near-field atmospheric inversions for the localization and quantification
863 Of controlled methane releases using stationary and mobile measurements. *Q. J. R. Meteorol. Soc.* 2022, 148,
864 1886–1912

865

866 Kissas K , Ibrom A , Kjeldsen P , et al. Methane emission dynamics from a Danish landfill: The effect of changes
867 in barometric pressure. *Waste Management*, 2022, 138:234-242.

868

869 Lian, J., Bréon, F.-M., Broquet, G., Lauvaux, T., Zheng, B., Ramonet, M., Xueref-Remy, I., Kotthaus, S.,
870 Haefelin, M., and Ciais, P.: Sensitivity to the sources of uncertainties in the modeling of atmospheric CO₂
871 concentration within and in the vicinity of Paris, *Atmos. Chem. Phys.*, 21, 10707–10726,
872 <https://doi.org/10.5194/acp-21-10707-2021>, 2021.

873

874 Lin, X., Zhang, W., Crippa, M., Peng, S., Han, P., Zeng, N., Yu, L., and Wang, G.: A comparative study of
875 anthropogenic CH₄ emissions over China based on the ensembles of bottom-up inventories, *Earth Syst. Sci. Data*,
876 13, 1073–1088, <https://doi.org/10.5194/essd-13-1073-2021>, 2021.

877

878 Lopez-Coto, I., Ren, X., Salmon, O. E., Karion, A., Shepson, P. B., Dickerson, R. R., Stein, A., Prasad, K., and
879 Whetstone, J. R.: Wintertime CO₂, CH₄, and CO Emissions Estimation for the Washington, DC-Baltimore
880 Metropolitan Area Using an Inverse Modeling Technique, *Environmental Science and Technology*, 54, 2606–2614,
881 <https://doi.org/10.1021/acs.est.9b06619>, 2020.

882

883 Lou, Z., Cai, B.F., Zhu, N., Zhao, Y., Geng, Y., Yu, B., Chen, W., Greenhouse gas emission inventories from waste

884 sector in China during 1949–2013 and its mitigation potential. *J. Clean. Prod.* 157, 118–124.
885 <https://doi.org/10.1016/j.jclepro.2017.04.135>, 2017.

886

887 Lu, X., Jacob, D. J., Zhang, Y., Maasackers, J. D., Sulprizio, M. P., Shen, L., Qu, Z., Scarpelli, T. R., Nesser, H.,
888 Yantosca, R. M., Sheng, J., Andrews, A., Parker, R. J., Boesch, H., Bloom, A. A., and Ma, S.: Global methane
889 budget and trend, 2010–2017: complementarity of inverse analyses using in situ (GLOBALVIEW-
890 ObsPack) and satellite (GOSAT) observations, *Atmos. Chem. Phys.*, 21, 4637–4657, [https://doi.org/10.5194/acp-](https://doi.org/10.5194/acp-21-4637-2021)
891 [21-4637-2021](https://doi.org/10.5194/acp-21-4637-2021), 2021.

892

893 Kaiho K., Koga S. Impacts of a massive release of methane and hydrogen sulfide on oxygen and ozone during the
894 late Permian mass extinction. *Global Planetary Change*, 107:91-101,
895 <https://doi.org/10.1016/j.gloplacha.2013.04.004>, 2013.

896

897 Maasackers, J. D., Varon, D. J., Elfarisdóttir, A., McKeever, J., Jervis, D., Mahapatra, G., Pandey, S., Lorente, A.,
898 Borsdorff, T., Foorhuis, L. R., Schuit, B. J., Tol, P., van Kempen, T. A., van Hees, R., & Aben, I. Using satellites to
899 uncover large methane emissions from landfills. *Sci. Adv.* 8, eabn9683, 10.
900 <https://doi.org/10.1126/sciadv.abn9683>, 2022.

901

902 Masuda, S., Sano, I., Hojo, T., Li, Y., Nishimura, O., The comparison of greenhouse gas emissions in sewage
903 treatment plants with different treatment processes. *Chemosphere* 193, 581–590, 2018.

904

905 Miles, N. L., Richardson, S. J., Lauvaux, T., Davis, K. J., Balashov, N. V., Deng, A., Turnbull, J. C., Sweeney, C.,
906 Gurney, K. R., Patarasuk, R., Razlivanov, I., Cambaliza, M. O. L. and Shepson, P. B.: Quantification of urban
907 atmospheric boundary layer greenhouse gas dry mole fraction enhancements in the dormant season: Results from
908 the Indianapolis Flux Experiment (INFLUX), *Elem Sci Anth*, 5, 27, doi:10.1525/elementa.127, 2017.

909

910 Miller, S. M., Matross, D. M., Andrews, A. E., Millet, D. B., Longo, M., Gottlieb, E. W., Hirsch, A. I., Gerbig, C.,
911 Lin, J. C., Daube, B. C., Hudman, R. C., Dias, P. L. S., Chow, V. Y., and Wofsy, S. C.: Sources of carbon monoxide
912 and formaldehyde in North America determined from high-resolution atmospheric data, *Atmos. Chem. Phys.*, 8,
913 7673–7696, <https://doi.org/10.5194/acp-8-7673-2008>, 2008.

914

915 Miller, S. M., Michalak, A. M., Detmers, R. G., Hasekamp, O. P., Bruhwiler, L. M. P., & Schwietzke, S. China's
916 coal mine methane regulations have not curbed growing emissions. *Nature Communications*, 10(1), 303–308.
917 <https://doi.org/10.1038/s41467-018-07891-7>, 2019.

918 Mønster, J., Kjeldsen, P. and Scheutz, C. (2019) Methodologies for measuring fugitive methane emissions from
919 landfills – a review. In *Waste Management.*, 87, 835– 859. <https://doi.org/10.1016/j.wasman.2018.12.047>.

920 National Bureau of Statistics of China (NBSC), *China Statistical Yearbook* (China Statistics Press, 2015) (in
921 Chinese).

922

923 Pak N M , Heerah S , Zhang J , et al. The Facility Level and Area Methane Emissions inventory for the Greater
924 Toronto Area (FLAME-GTA)[J]. *Atmospheric Environment*, 2021, 252(9):118319.

925

926 Peng, S., Piao, S., Bousquet, P., Ciais, P., Li, B., Lin, X., Tao, S., Wang, Z., Zhang, Y., and Zhou, F.: Inventory of

927 anthropogenic methane emissions in mainland China from 1980 to 2010, *Atmos. Chem. Phys.*, 16, 14545–14562,
928 <https://doi.org/10.5194/acp-16-14545-2016>, 2016.

929

930 Sargent, M., Barrera, Y., Nehrkorn, T., Hutyra, L. R., Gately, C. K., Mckain, K., Sweeney, C., Hegarty, J.,
931 Hardiman, B., Steven C. Wofsy, S. C.: Anthropogenic and biogenic CO₂ fluxes in the Boston urban region, *P. Natl.*
932 *Acad. Sci. USA.*, 115(40), <https://doi.org/10.1073/pnas.1803715115>, 2018.

933

934 Saunio, M., Stavert, A. R., Poulter, B., et al., The Global Methane Budget 2000–2017, *Earth Syst. Sci. Data*, 12,
935 1561–1623, <https://doi.org/10.5194/essd-12-1561-2020>, 2020.

936

937 Seto, K. C. hakal, S. Bigio, A. Blanco, H. elgado, G. C. ewar., Huang, L. Inaba, A. Kansal, A. Lwasa, S. cahon, J.
938 ller., B. urakami, J. Nagendra, H. amaswami, A. Humansettlements, infrastructure and spatial planning. *Climate*
939 *Change 2014: Mitigation of Climate Change. IPCC Working Group III Contribution to AR5*; Cambridge University
940 Press, 2014; Chapter 12.

941

942 Solazzo, E., Crippa, M., Guizzardi, D., Muntean, M., Choulga, M., and Janssens-Maenhout, G.: Uncertainties in
943 the Emissions Database for Global Atmospheric Research (EDGAR) emission inventory of greenhouse gases,
944 *Atmos. Chem. Phys.*, 21, 5655–5683, <https://doi.org/10.5194/acp-21-5655-2021>, 2021.

945

946 Spokas, K.A., et al. 2021. Modeling landfill CH₄ emissions: CALMIM international field validation, using
947 CALMIM to simulate management strategies, current and future climate scenarios. *Elem Sci Anth*, 9: 1.
948 <https://doi.org/10.1525/elementa.2020.00050Do>, 2020.

949

950 Tolaymat, T., M., R. B. Green, G. R. Hater, M. A. Barlaz, P. Black, D. Bronson, J. Powell, Evaluation of landfill
951 gas decay constant for municipal solid waste landfills operated as bioreactors. *J. Air Waste Manage. Assoc.* 60, 91–
952 97, 2010.

953

954 Thoning, K. W., Tans, P. P., and Komhyr, W. D.: Atmospheric carbon dioxide at Mauna Loa observatory 2.
955 Analysis of the NOAA/GMCC data, 1974–1985, *J. Geophys. Res.-Atmos.*, 94, 8549–
956 8565, <https://doi.org/10.1029/JD094iD06p08549>, 1989.

957 Tian, J., Gong, Y., Li, Y., Chen, X., Zhang, L., & Sun, Y. (2022). Can policy implementation increase public waste
958 sorting behavior? The comparison between regions with and without waste sorting policy implementation in China.
959 *Journal of Cleaner Production*, 132401.

960

961 United States Environmental Protection Agency (USEPA), Global Mitigation of Non-CO₂ Greenhouse Gases
962 2010-2030 (United States Environmental Protection Agency Office of Atmospheric Programs (6207J),
963 EPA-430-R-13-011, 2013);
964 www.epa.gov/sites/production/files/2016-07/documents/mac_report_2014-exec_summ.compressed.pdf

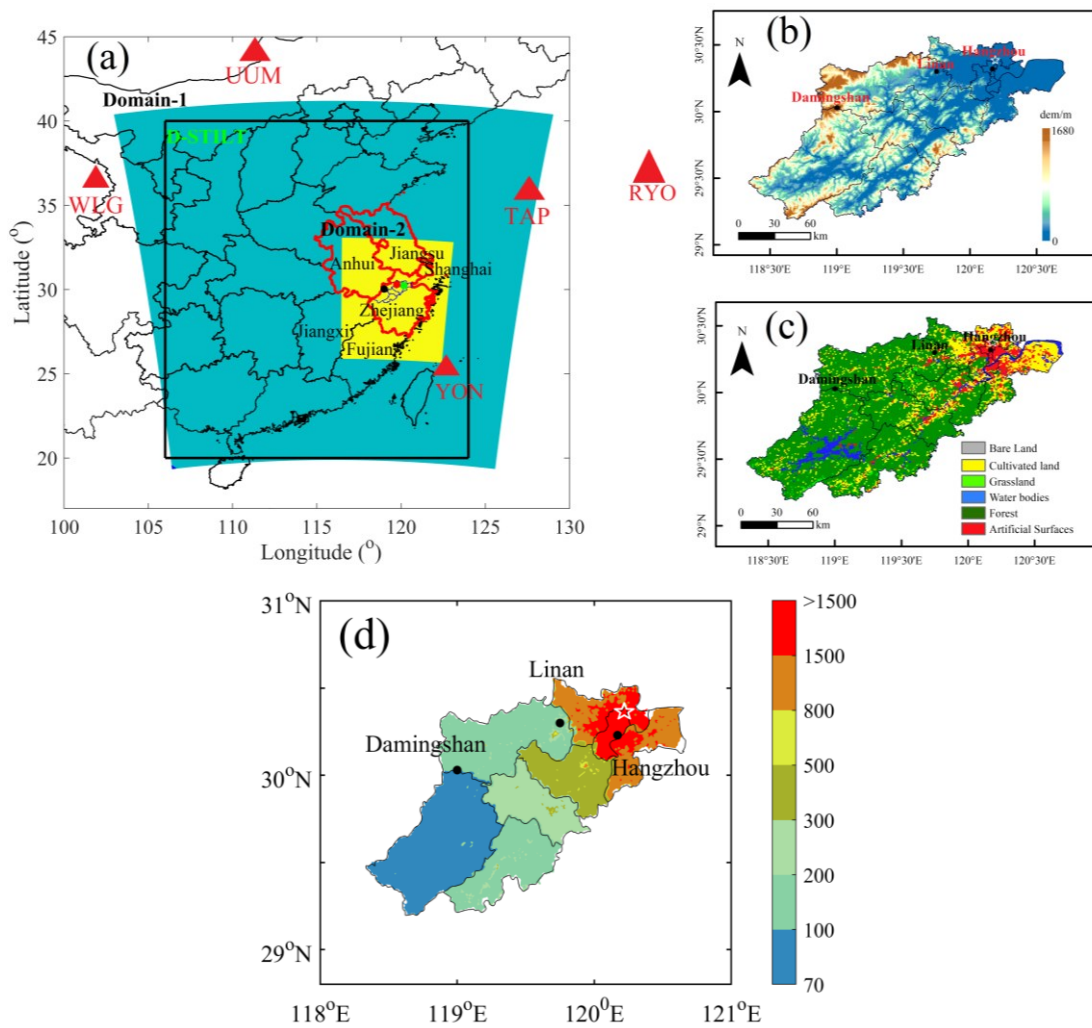
965 Verhulst, K. R., Karion, A., Kim, J., Salameh, P. K., Keeling, R. F., Newman, S., Miller, J., Sloop, C., Pongetti, T.,
966 Rao, P., Wong, C., Hopkins, F. M., Yadav, V., Weiss, R. F., Duren, R. M. and Miller, C. E.: Carbon dioxide and
967 methane measurements from the Los Angeles Megacity Carbon Project – Part 1: calibration, urban enhancements,
968 and uncertainty 10 estimates, *Atmos. Chem. Phys.*, 17(13), 8313–8341, doi:10.5194/acp-17-8313-2017, 2017

969 Wang, X., A. S. Nagpure, J. F. DeCarolis, M. A. Barlaz, Characterization of uncertainty in estimation of methane
970 collection from select U.S. landfills. *Environ. Sci. Technol.* 49, 1545–1551, 2015.
971
972 Wang, Y., Wang, X., Wang, K. *et al.* The size of the land carbon sink in China. *Nature*, E7–E9.
973 <https://doi.org/10.1038/s41586-021-04255-y>, 2022.
974
975 Williams, J. P., Ars, S., Vogel, F., Regehr, A., & Kang, M. (2022). Differentiating and Mitigating Methane
976 Emissions from Fugitive Leaks from Natural Gas Distribution, Historic Landfills, and Manholes in Montréal,
977 Canada. *Environmental Science & Technology*. <https://doi.org/10.1021/acs.est.2c06254>
978
979 Yadav, V., Duren, R., Mueller, K., Verhulst, K. R., Nehrkorn, T., and Kim, Jet., Spatio-temporally resolved
980 methane fluxes from the Los Angeles megacity *J. Geophys. Res. Atmos.* 124, 5131–5148 (2019).
981
982 Zhao, X., Jin, X., Guo, W., Zhang, C., Shan, Y., Du, M., Tillotson, M., Yang, H., Liao, X., and Li, Y.: China's
983 urban methane emissions from municipal wastewater treatment plant, *Earths Future*, 7, 480–490, 2019.
984
985 Zhao, Z., Bian, R., Zhao, F., Chai, X., Implications of municipal solid waste disposal methods in China on
986 greenhouse gas emissions. *Renew. Sust. Energ. Rev.* 39 (3). <https://doi.org/10.1002/ep.13372>, 2019.
987
988 Zhang, B. and Chen, G.: China's CH₄ and CO₂ emissions: Bottomup estimation and comparative analysis, *Ecol.*
989 *Indic.*, 47, 112– 122, <https://doi.org/10.1016/j.ecolind.2014.01.022>, 2014.
990
991 Zhang, K., Lee, X., Schultz, N. M., Huang, Q., Liu, Z., Chu, H., Zhao, L., & He, C. A global dataset on subgrid
992 land surface climate (2015-2100) from the Community Earth System Model. *Geosci. Data J.*, 1–12.
993 <https://doi.org/10.1002/gdj3.153>, 2022.

994 Zhang Y., Fang S., Chen J., Lin Y., Chen Y., Liang R., Jiang K., Parker R., Boesch H., Steinbacher M., Sheng J.,
995 Lu X., Shaojie Song, Shushi Peng: Observed Changes in China's Methane Emissions Linked to Policy Drivers,
996 *Proceedings of the National Academy of Sciences*, 119, e2202742119, 2022.

997 Zhejiang Provincial Bureau of Statistics, Survey Office of the National Bureau of Statistics in Zhejiang, Zhejiang
998 Statistical Yearbook 2018-2019 (China Statistics Press, Beijing, China, 2019)

999
1000
1001
1002
1003
1004
1005



1006

1007

1008 Figure 1. (a) WRF-STILT model domain setups, three CH₄ concentration observation sites in
 1009 Hangzhou city, and five CH₄ background sites, note the green, red and black dots represent
 1010 locations for Hangzhou site, Linan site and Damingshan site, respectively, Yangtze River Delta
 1011 regions is displayed in red boundary, back rectangle represents domain in STILT model, (b)
 1012 geophysical height within Hangzhou city, (c) land surface categories in Hangzhou city, and (d)
 1013 population density in Hangzhou city for year 2019, units: person per km², the location of landfills
 1014 in Hangzhou city is displayed with a white star.

1015

1016

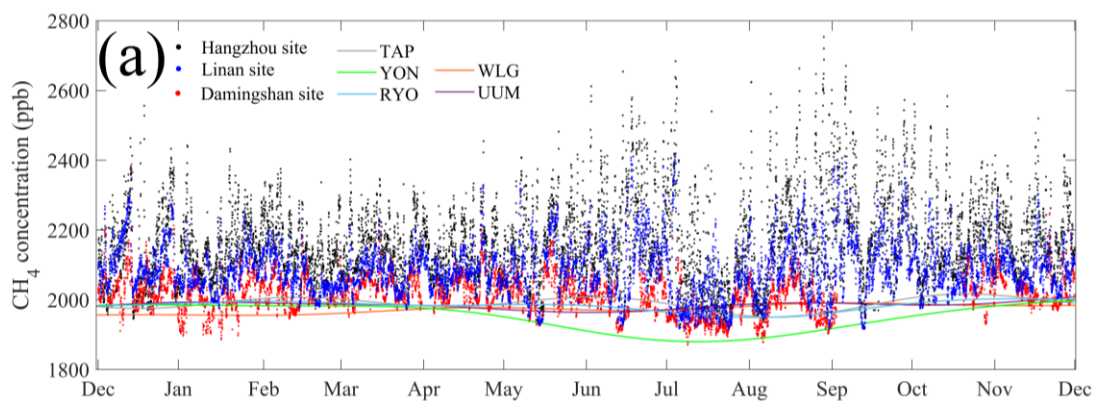
1017

1018

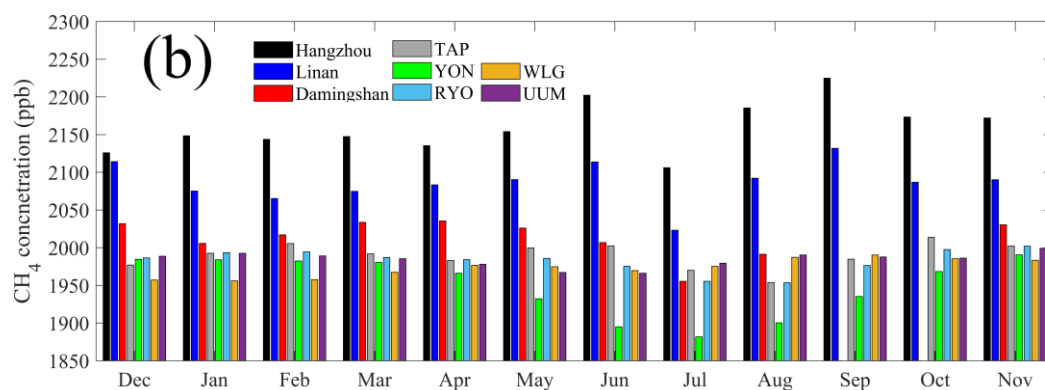
1019

1020

1021



1022



1023

1024

1025

1026

1027

1028

1029

1030

1031

1032

1033

1034

1035

1036

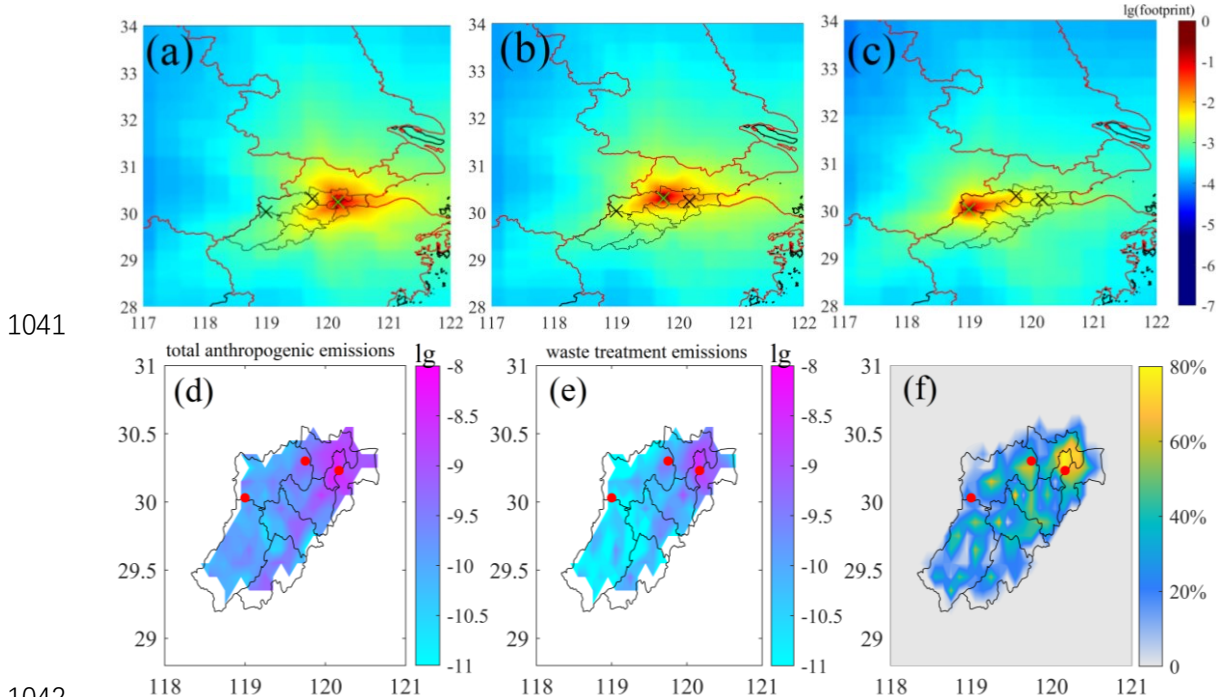
1037

1038

1039

1040

Figure 2. (a) Hourly CH₄ concentrations at three sites within Hangzhou city as Hangzhou site, Linan site, and Damingshan site, and fitting CH₄ background based on CCGCRV regression method at five background sites as TAP, YON, RYO, WLG and UUM, (b) monthly mean of CH₄ concentrations for above eight sites. Note the CH₄ background is smoothed by using CCGCRV fitting method on weekly or hourly observations, which can filter large fluctuations caused by sudden and unidentified sources



1041

1042

1043

1044

1045

1046

1047

1048

1049

1050

1051

1052

1053

1054

1055

1056

1057

1058

1059

1060

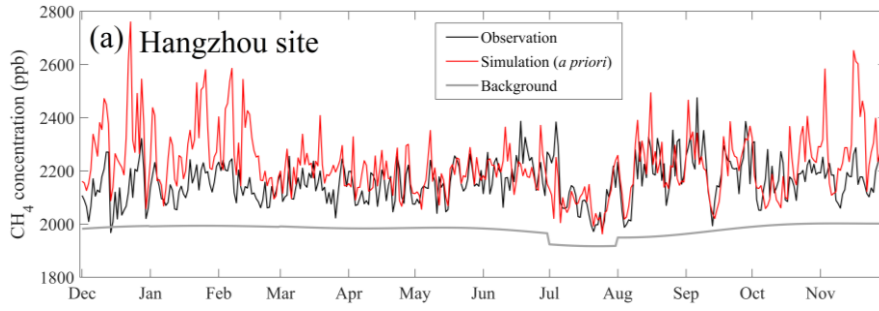
1061

1062

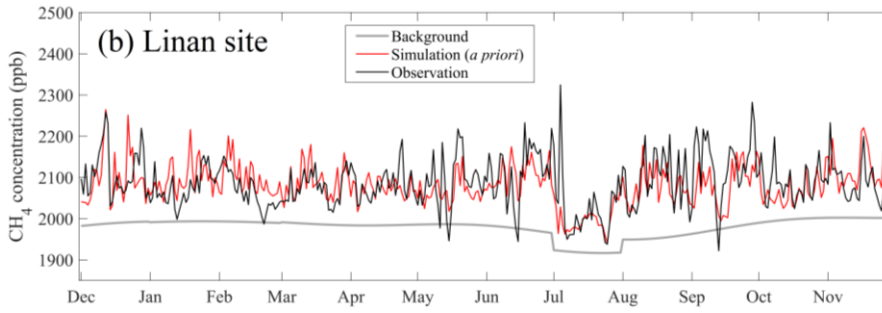
1063

1064

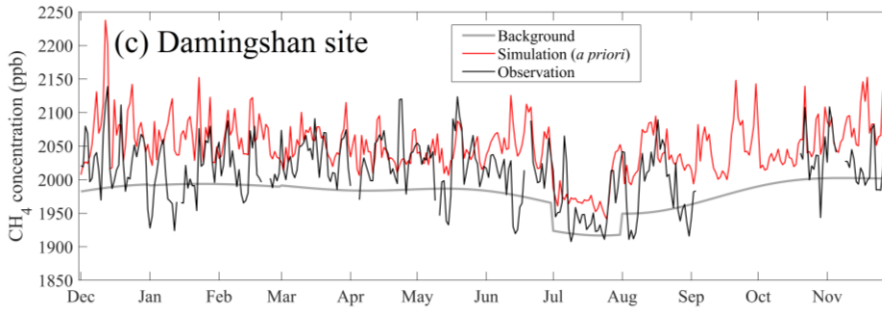
Figure 3. Annual averages of simulated footprint for (a) Hangzhou site, (b) Linan site, and (c) Damingshan site, where the green symbol “×” indicates receptor location in each pannel, (d) total anthropogenic CH₄ emissions in EDGAR v6.0 inventory, (e) waste treatment CH₄ emissions in EDGAR v6.0 inventory, and (f) proportions of waste treatment to total anthropogenic CH₄ emissions, red dot represents three sites, units for footprint: ppm m² s mol⁻¹, units for emissions: kg m² s⁻¹. The divisions in Hangzhou city are different districts.



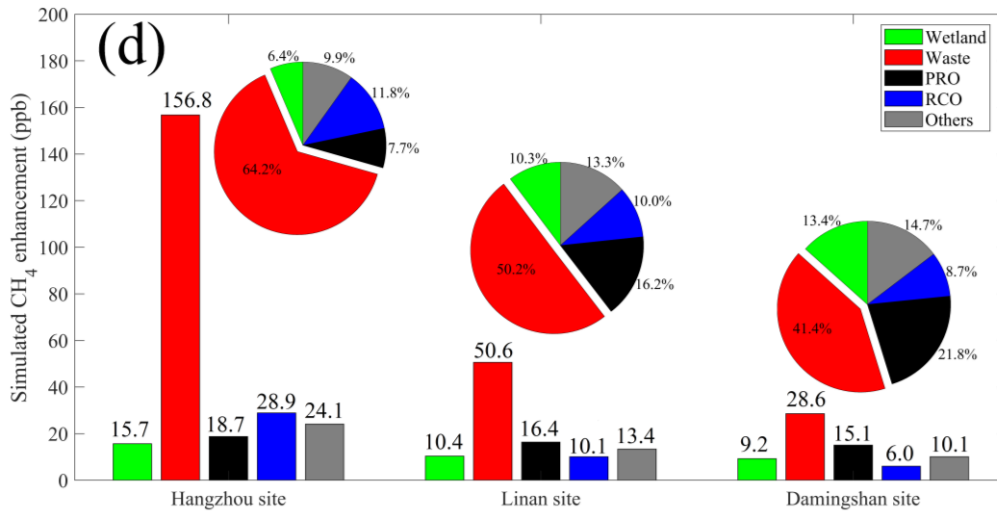
1065



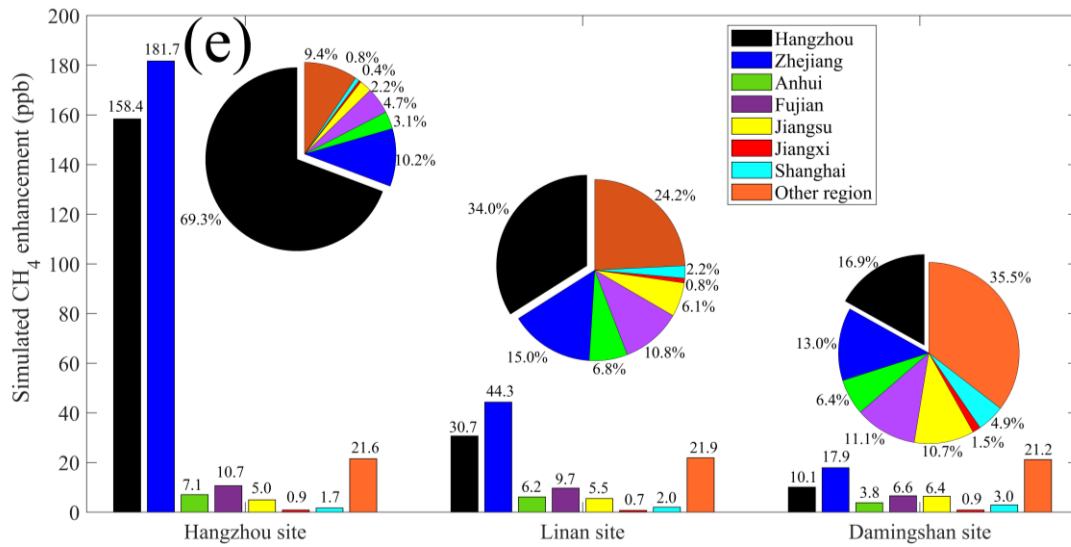
1066



1067



1068



1069

1070 Figure 4. Comparisons between daily CH₄ observations and simulations for (a) Hangzhou site, (b)
 1071 Linan site, (c) Damingshan site, (d) simulated CH₄ enhancements from main emission categories
 1072 (e) simulated anthropogenic CH₄ enhancement from different regions and its proportions. Note the
 1073 blue color for the bar charts include all contributions from “Zhejiang”, including “Hangzhou”; and the
 1074 blue regions in the pie charts represent rest regions of “Zhejiang minus Hangzhou”.

1075

1076

1077

1078

1079

1080

1081

1082

1083

1084

1085

1086

1087

1088

1089

1090

1091

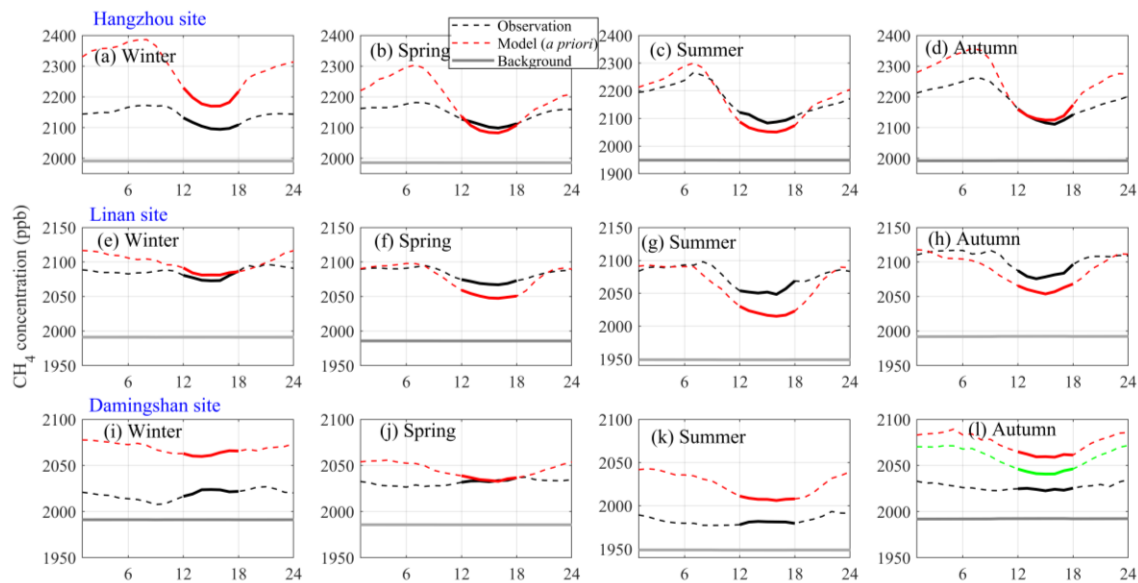
1092

1093

1094

1095

1096



1097

1098 Figure 5. Seasonal averaged diurnal variations for Hangzhou site in (a) winter, (b) spring, (c)
 1099 summer, (d) autumn, and Linan site in (e) winter, (f) spring, (g) summer, (h) autumn, and
 1100 Damingshan site in (i) winter, (j) spring, (k) summer, (l) autumn; Note because of two months of
 1101 data gap in Autumn for Damingshan site, the green line is for all September-November
 1102 simulations, red line only represent simulation of corresponding period for available observation
 1103 data, and bold lines represents data between 12:00 and 18:00.

1104

1105

1106

1107

1108

1109

1110

1111

1112

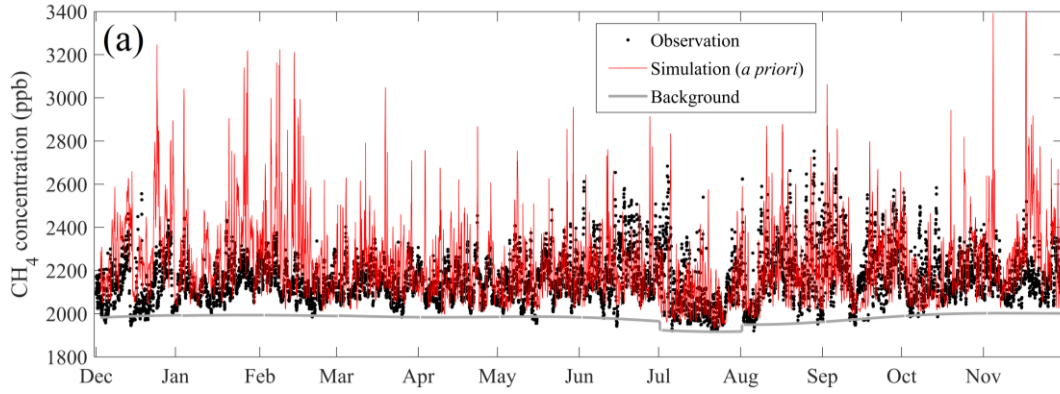
1113

1114

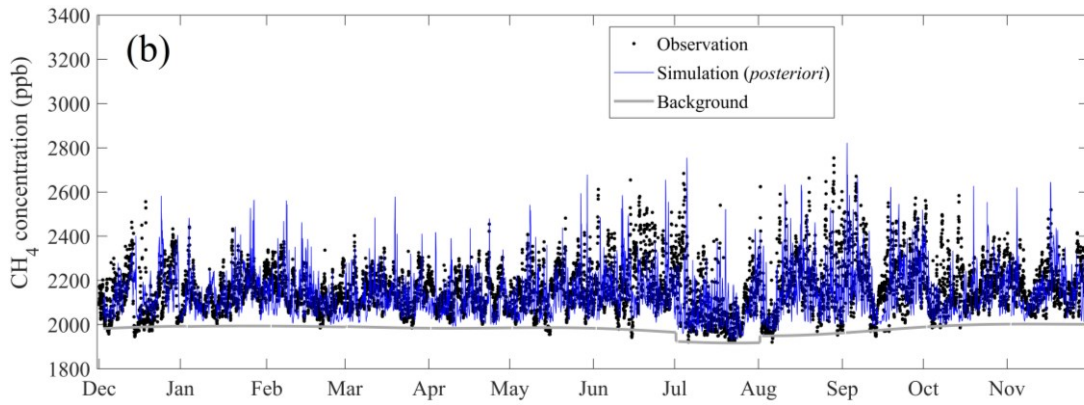
1115

1116

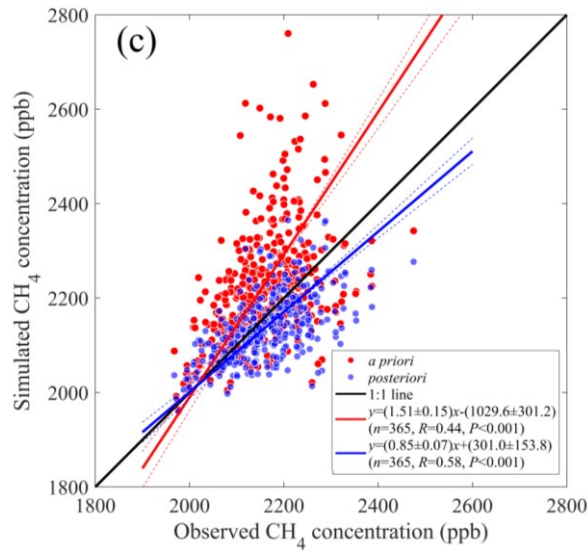
1117



1118



1119



1120

1121 Figure 6. Comparisons of hourly CH₄ concentrations at Hangzhou site between observations and
 1122 simulations by using (a) *a priori* and (b) *posteriori* emissions, (c) scatter plots of daily CH₄
 1123 averages by using *a priori* and *posteriori* emissions.

1124

1125

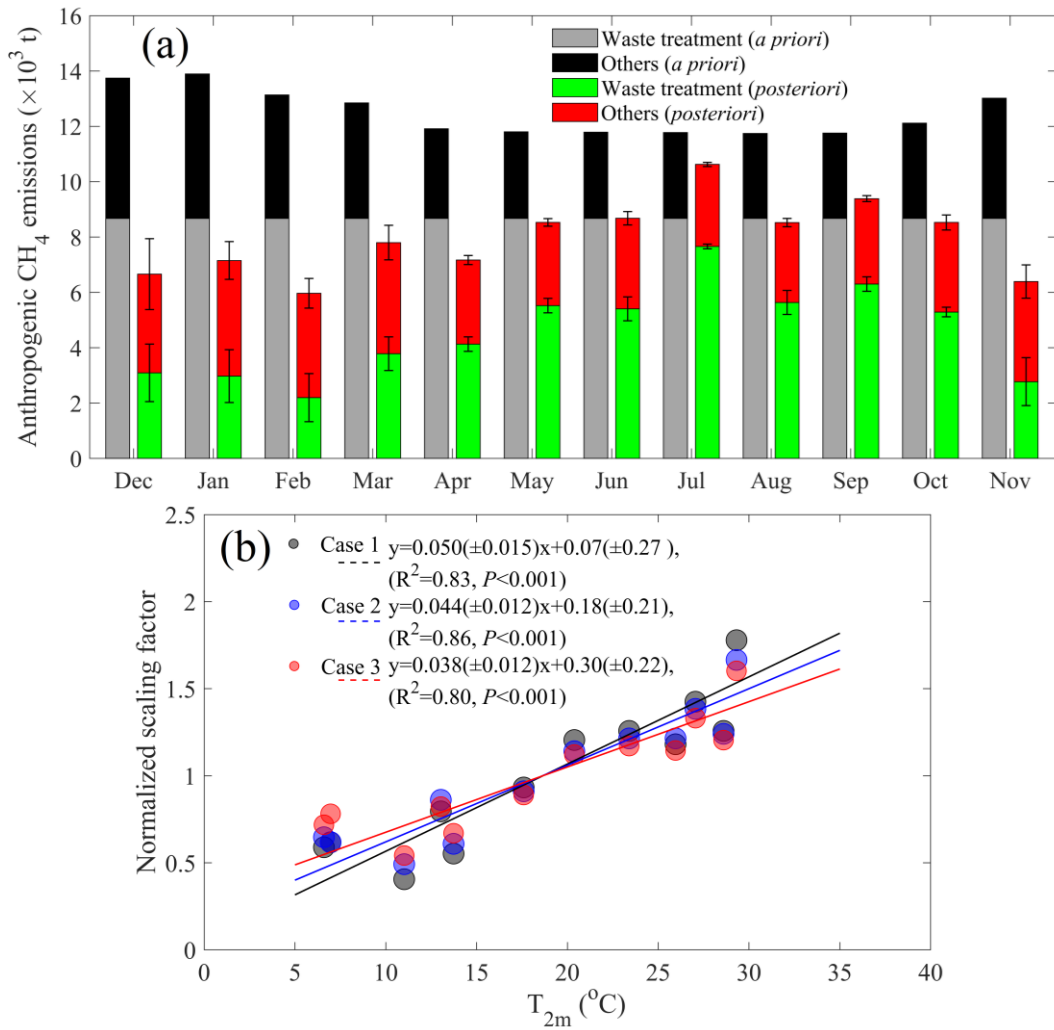
1126

1127

1128

1129

1130



1131

1132

1133

1134

1135

1136

1137

1138

1139

1140

1141

1142

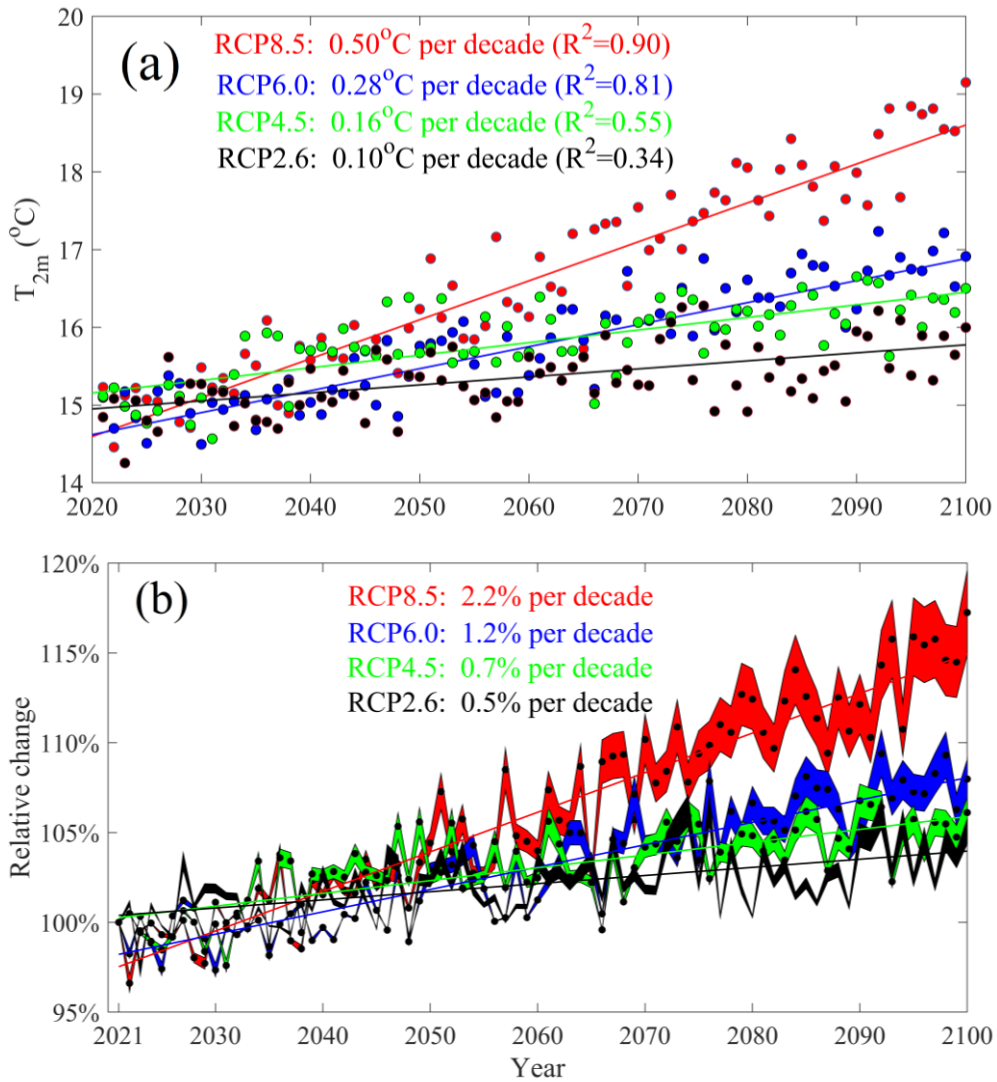
1143

1144

1145

1146

Figure 7. (a) Monthly anthropogenic (excluding agricultural soil) CH₄ emissions for *a priori* and *posteriori* emissions for Hangzhou city, (b) relationship between the monthly *posteriori* CH₄ emissions and temperature for the three cases discussed in section 2.3 of this text.



1147

1148

1149 Figure 8. (a) Annual air temperature from year 2021 to 2100 for four different global warming
 1150 scenarios for Hangzhou city, (b) the projected relative change of waste treatment CH_4 emissions
 1151 (or EFs) for Hangzhou city, note the shading indicates extent of three cases.

1152

1153

1154

1155

1156

1157

1158

1159

1160

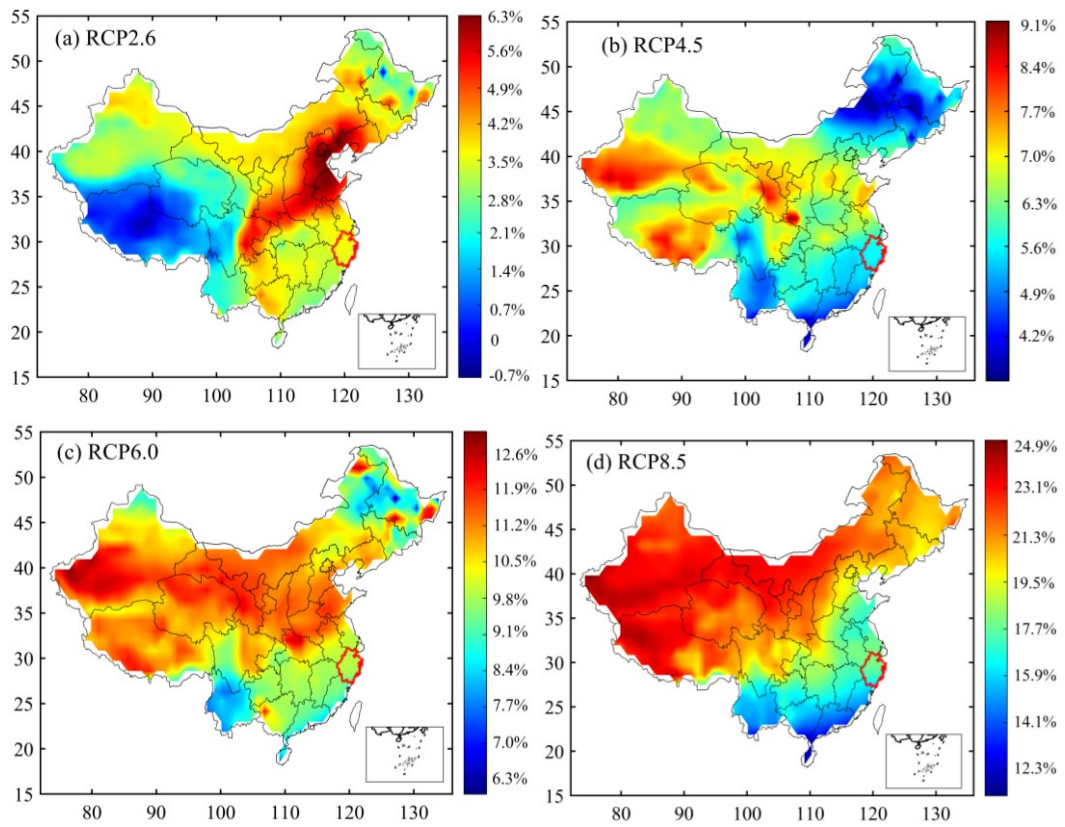
1161

1162

1163

1164

1165



1166

1167

1168

1169

1170

1171

1172

1173

1174

1175

1176

1177

1178

1179

1180

1181

1182

1183

1184

1185

1186

1187

1188

1189

1190

1191

Figure 9. Global warming induced relative changes of waste treatment CH₄ EFs by year of 2100 for (a) RCP2.6, (b) RCP4.5, (c) RCP6.0, and (d) RCP8.5 scenarios. Note the red boundary is Zhejiang province.

1192 Table 1. The *posteriori* SFs for different categories in three cases for Hangzhou city, where
 1193 wetland: natural and agricultural wetland, Waste: waste treatment, PRO: fuel exploitation, RCO:
 1194 energy for building, Others: the rest anthropogenic emissions. Note Case 1: 3 categories, and 300%
 1195 uncertainty for waste treatment; Case 2: 5 categories; Case 3: 3 categories, and 200% uncertainty
 1196 for waste treatment.

Mont h	Case 1			Case 2					Case 3		
	Wetland	Waste	Others	Wetland	Waste	PRO	RCO	Others	Wetland	Waste	Others
1	1.00	0.29	0.83	1.00	0.34	0.90	0.80	0.93	1.00	0.40	0.72
2	1.00	0.20	0.89	1.00	0.26	0.97	0.83	0.93	1.00	0.30	0.77
3	1.03	0.39	1.04	1.02	0.46	1.07	0.80	0.97	1.02	0.46	0.95
4	1.10	0.46	0.96	1.08	0.48	1.01	0.95	0.93	1.08	0.49	0.91
5	1.12	0.62	0.99	1.10	0.64	1.06	0.97	0.92	1.11	0.65	0.95
6	1.22	0.59	1.09	1.18	0.64	1.05	0.97	1.03	1.18	0.64	1.05
7	1.10	0.88	0.96	1.09	0.88	1.00	1.00	0.94	1.09	0.89	0.94
8	1.05	0.62	0.95	1.01	0.66	0.99	0.97	0.95	1.01	0.67	0.91
9	1.04	0.71	1.01	1.02	0.73	0.96	0.98	1.04	1.02	0.74	0.98
10	1.06	0.60	0.94	1.06	0.61	0.92	0.96	1.00	1.06	0.62	0.90
11	1.01	0.27	0.86	1.00	0.32	0.91	0.85	0.93	1.00	0.37	0.75
12	1.00	0.31	0.70	1.00	0.33	0.75	0.79	0.91	1.00	0.43	0.58

1197
 1198
 1199
 1200
 1201
 1202
 1203
 1204
 1205
 1206
 1207
 1208
 1209
 1210
 1211
 1212